Do badlands (always) control sediment yield? Evidence from a small intermittent catchment

Llena M.[1,*], Batalla R.J.[1,2,3], Smith, M.W.[4], Vericat D.[1,5]

[1] Fluvial Dynamics Research Group, Department of Environment and Soil Sciences, University of Lleida, Lleida, Spain.

[2] Catalan Institute for Water Research, Girona, Catalunya, Spain.

[3] Faculty of Forest Sciences and Natural Resources, Universidad Austral de Chile, Valdivia, Chile.

[4] School of Geography, University of Leeds, Leeds, UK.

[5] Forest Science and Technology Centre of Catalonia, Solsona, Spain.

* Corresponding author: mllena@macs.udl.cat

ABSTRACT

The objective of this paper is to analyse the sediment production and the sediment yield in a small mountain catchment (10 km^2) characterised by patches of badlands (occupying 25% of the catchment area) and drained by intermittent streams located in the Southern Pyrenees. The study is performed at multiple temporal scales to further highlight: (i) the effect of pulses in the transfer of water and sediment; (ii) the contribution of the sediment production from badlands to the sediment yield of the catchment; and (iii) the role of the drainage network as sediment source and sink. Significant correlations between meteorological and flow variables were found; specifically, the strongest positive relations were observed between stream flashiness and the duration of the period in which the stream is dry, the sediment production and the suspended sediment concentration. Results indicated that badlands do not always control the export of sediments. At the annual scale, badlands supply around 54% of the total catchment sediment export. Seasonally, sediment produced in badlands can be higher than the amount exported at the catchment outlet. Materials transferred from agricultural fields and forest also contribute substantially to the sediment yield. Results emphasise the key role of the channel network on controlling pulses of sediment export, in direct relation to the intermittent character of the stream. The frequency and magnitude of such pulses determines the catchment Sediment Delivery Ratio (SDR), depending on whether the drainage network acts as a sediment sink (i.e. SDR < 1) or source (i.e. SDR > 1).

Key words: badlands, sediment production, sediment yield, flashiness, Sediment Delivery Ratio, flow intermittency.

1. INTRODUCTION

Plant cover, together with rainfall intensity and slope, are considered the most important factors controlling soil erosion (e.g. Borrelli et al., 2013; Cerovski-Darriau and Roering, 2016). *Badlands* are described as highly-dissected landscapes with little or no vegetation cover and high erosion rates (Yair et al., 1980; Clotet et al. 1987; Gallart et al 2002; Francke, 2009). They are frequently reported as being the main sediment source in catchments worldwide, notably in Mediterranean climate regions (e.g. Richard and Mathys 1999; Llorens et al., 2018). Besides badlands, agricultural areas are also important sediment sources, with moderate to high rates of soil erosion (e.g. Casalí et al., 2008), whereas forested areas present lower rates (e.g. Zabaleta et al., 2007). However, and despite the fact that these two types of surfaces typically display lower sediment production rates than those observed in badlands (e.g. Mathys et al., 2003; García-Ruíz et al., 2015; Llorens et al., 2018), they should not be dismissed in the estimation of sediments yields, especially in mountain regions where they usually cover large swathes of territory. Moreover, streamflow in catchments exhibiting patches of badlands is often intermittent and flashy (MacDonough et al., 2011), mostly due to the rapid concentration of surface runoff caused by the large presence of bare surfaces (e.g. Gallart and Llorens, 2004; García-Ruiz et al., 2008). These characteristics determine much of the transfer of water and sediments through the drainage network, which occur typically in the form of pulses (Junk et al., 1989) out-of-phase with hillslope sediment production and erosion (e.g. Puigdefabregas et al., 1999; Cui et al., 2003; Gran and Czuba, 2017).

Erosion rates in badlands have been mainly analysed by means of dynamic (i.e. sediment fluxes; e.g. Nadal-Romero et al., 2007; Mathys et al., 2003) and volumetric methods (i.e. topographic changes; Benito et al., 1992; Vericat et al., 2014). High Resolution Topography developed from advanced surveying platforms, sensors and algorithms (e.g. Structure from Motion photogrammetry, SfM), has permitted the quantification of topographic changes in different types of surfaces at high spatial and temporal resolutions (Tarolli, 2014; Passalacqua et al., 2015; Vericat et al., 2017), including badlands. Therefore, erosion rates and the subsequent sediment production of badland landscapes can be now inferred from topographic change detection at multiple temporal scales (e.g. Vericat et al., 2014; Stöcker et al., 2015; Smith and Vericat, 2015; Neugirg et al., 2016; Llena et al., under revision).

Most studies of sediment delivery from catchments patched with badlands focus on the sediment production from a specific area (e.g. Barnes et al., 2016; Benito et al., 1992), while others quantify the total sediment yield at the catchment outlet (e.g. Nadal-Romero et al., 2007;

Regüés et al., 1995). However, fewer studies encompass both type of analysis (e.g. Mathys et al., 2003; López-Tarazón et al., 2012). The integration of measurements at multiple temporal scales allows analysis of the role of specific sediment sources, such as the badlands, and their contribution to the total sediment yield for different time spans and in relation to meteorological and hydrological variables.

Moreover, it is worth noting the role of the drainage network (river channels) as a sediment sink and source, an element of riverscapes that is often neglected from sediment budgets, especially in small mountain areas, where channel related processes are seemingly less evident. For instance, López-Tarazón et al. (2011) examined the contribution of badlands to the sediment yield of the meso-scale Isábena catchment in the Southern Pyrenees. Although virtually all of the sediments at the outlet of the catchment were produced and eroded from the sub-catchments draining badlands, the channel network acted as source and sink of these sediments, controlling the dynamics observed at the outlet. López-Tarazón et al. (2011) concluded that, annually, all sediments were exported (i.e. Sediment Delivery Ratio around 1) but with marked seasonal changes, implying sedimentation and erosion of fine sediment in the channel bed. This type of integrated analysis is key to catchment-to-stream management, especially in rivers that present acute flashiness behaviour (e.g. flash floods; e.g. Marchi et al., 2010; Tarolli et al., 2012; Surian et al., 2016; Amponsah et al., 2016), high sediment yields (e.g. reservoir siltation, Martínez-Casasnovas and Poch, 1998), and reduced water quality (e.g. high sediment concentrations and load, Pimentel et al., 1995).

Within this context, this paper aims to analyse the sediment production and sediment yield in a small mountain catchment characterised by patches of badlands and drained by intermittent streams. The study is performed at multiple temporal scales in order to further highlight: (i) the effect of specific pulses in the transfer of water and sediment; ii) the contribution of the sediment production from badlands to the sediment yield at the catchment outlet; and (iii) the role of the drainage network as a sediment source and sink. Additionally, statistical correlations between meteorological, sediment and flow variables are investigated. The working hypothesis, based on initial field observations of badlands' responses in the study area is that, despite their high sediment production, badlands do not fully control the catchment's sediment yield, nor do they completely explain the seasonal variability of it. We further hypothesize that the role of the drainage network is key to understanding the sediment transfer in these type of catchments, which are typically dominated by intermittent flashy streams.

2. STUDY AREA

The River Soto is a tributary of the Upper River Cinca (Central Pyrenees, Ebro basin, Iberian Peninsula; Figure 1A). This is a small mountain catchment (i.e. 10 km^2) with an altitude range from 540 m a.s.l. at the outlet to 1047 m a.s.l. in the headwaters. Eocene grey marls with different degree of compactness and harder layers of sandstones underlay most part of the catchment. Due to the high erodibility of these materials, the study area is characterized by a dense network of badlands that occupy the 25% of the catchment's area. The remainder of the catchment is covered by Mediterranean forest (56%; mainly *Pinus halepensis*) and winter cereal (18%). The catchment has a continental Mediterranean climate with a mean annual rainfall of 755 mm (period 1981-2018). Maximum rainfall intensities are observed in spring and autumn, occasionally attaining 50 mm h^{-1}. Mean annual temperature is 13°C, ranging from -6°C and to 37°C (daily values). During winter, temperatures below freezing are often registered (on average, 60 days every year are exposed to temperatures <0ºC). The flow regime is intermittent (according to the classification by McDonough et al., 2011) with the stream normally drying out during August and September. Average daily discharge was 0.05 $m^3\ s^{-1}$ during the study period (2016-2018; no further data is available since the river was previously ungauged). The streamflow is characterized by the succession of flash floods with an average of 30 events per year (according to data between 2016 and 2018). Flash-floods typically last for one day and occur following intense thunderstorms (e.g. >25 mm accumulated rainfall). The low degree of forest cover and the high erosion rates of bare surface areas (badlands) means that during floods, the river transports large amounts of sediment (in suspension) to the River Cinca that immediately drains into the Mediano Reservoir (435 hm^3, in operation since 1974).

3. METHODS

3.1. Data acquisition and treatment

The study period covers two years, from July 2016 to June 2018. Three types of data were obtained: (i) meteorological data (rainfall and air temperature); (ii) sediment production from two experimental badlands through repeated high resolution topographic surveys; and (iii) water and sediment fluxes at the outlet of the catchment. Rainfall, air temperature, discharge and suspended sediment concentrations were acquired continuously, while topographic surveys were performed seasonally. Specifically, surveys were undertaken in the middle of summer, at the end of autumn and at the beginning of spring, yielding a total of six *seasonal* study periods

(Table 1). This allowed the study of the effect of distinct seasonal climatic characteristics (e.g. rainstorms in spring and summer, temperatures below 0ºC in winter) on weathering and erosion processes. Note that the summer seasons are included in the spring and autumn periods defined here (Table 1).

3.1.1. Rainfall and temperature

Rainfall and temperature were obtained from an *in-situ* meteorological station (see Figure 1A for location details). Rainfall was measured continuously by means of a Campbell ARG100® tipping bucket rain gauge, while air temperature was recorded by a Campbell Temperature Probe-109®. All data were recorded in the same data logger (Campbell CR200X®) at a 5-min interval. There is a significant relationship between these recorded values and the nearest meteorological stations (5 and 10 km away, respectively) operated by the Ebro Water Authorities (i.e. r^2=0.91, p<0.01), hence justifying the use of a single station to characterise the whole study catchment.

3.1.2. Sediment production from badlands

The sediment production from badlands was detailed by Llena et al. (under revision) from the comparison of repeat High Resolution Topography in two representative badlands of the study area. Despite the two monitored badlands having the same lithology, each one presented a specific morphometry (i.e. slope, aspect, network pattern) and vegetation cover, thereby encompassing the influence of morphometric and land cover characteristics on geomorphic processes re-shaping the badlands and, consequently, sediment production (e.g. Yair et al. 1980; Nadal-Romero et al 2007; Vericat et al. 2014; Marchamalo et al. 2016; Vergari et al., 2019). In this way, these surveyed badlands are representative of all the badlands in the study catchment. More information about the experimental badland can be also obtained at https://sites.google.com/site/badlandscan/. Specific details of both badlands are described in Llena et al. (under revision), but a summary of the methods is presented here.

Topographic surveys were performed by means of Structure from Motion (SfM) photogrammetry. Around 650 pictures per campaign and site were taken using a Panasonic Lumix DMC-TZ60® compact camera (focal length 4 mm which is a 35-mm equivalent of 25 mm; 10 Mpx) mounted on a 10-m telescopic inspection pole. SfM processing was implemented using standard workflows within Agisoft Photoscan Professional® 1.3.4. Dense point clouds with an average point density of around 5×10^4 observations m^{-2} (i.e. 5 obs cm^{-2}) were obtained. In terms of georeferencing and scaling, SfM data sets were registered by a floating control network of around 30 Ground Control Points (GCPs) per badland, set up based on a permanent network control. GCPs were spatially distributed, with an average mean absolute error of 0.023 m. In terms of quality assessment, an independent validation dataset of around 300 Check Points (ChPs) per survey was obtained with an average mean absolute error of 0.021 m. Point clouds were filtered to remove outliers and vegetation. The open-source Topographic Point Cloud Analysis Toolkit (ToPCAT; Brasington et al., 2012; Rychkov et al., 2012) was then used to regularize the point cloud (implemented in the Topographic Analysis Tools Software (TAT) extension for ArcMap®, available at http://tat.riverscapes.xyz/). A 0.05 × 0.05 m grid was selected, taking into account the magnitude of the topographic changes on the study area and the size of the smallest geomorphic features observed in the field (e.g. rills). ToPCAT allows the analysis of topographic data within each grid cell and calculation of a series of sub-grid statistics (e.g. maximum, mean and minimum elevations and detrended standard deviation of elevations). The minimum elevation within each cell was used to represent the ground elevation. A Triangular Irregular Network (TIN) was calculated based on these observations for each survey. Finally, a 0.05 m resolution DEM from each TIN was obtained.

Topographic changes were estimated by the comparison of DEMs between surveys (DEM of Differencing; i.e. DoD). DoDs were calculated by the Geomorphic Change Detection 7.4 (GCD) extension for ArcMap® (available at http://gcd.joewheaton.org/; see Wheaton et al. 2010). GCD also allows adding uncertainty analysis based on simple minimum Level of Detection (minLoD), propagating errors and performing probabilistic thresholding. The assessment of the spatially distributed uncertainty was addressed by the application of a Fuzzy Inference System (FIS) to consider errors from different sources (Wheaton et al., 2010). In this study we have used a modification of the FIS model proposed by Rossi (2018), which takes into account the slope and the roughness as the main factors determining the vertical uncertainty in SfM topographic datasets. A critical *t*-value at a confidence interval of 85% (i.e. the default value in GCD) was applied to calculate the spatially distributed minLoD (e.g. Brasington et al., 2000; Lane et al., 2003; Smith and Vericat, 2015). Those DoD cells with absolute values below the minLoD were considered uncertain and hence were not used in the computation of the thresholded DoDs.

The measured net topographic changes in the two study badlands were extrapolated to all the surface occupied by badlands in the study area; this was performed by multiplying the average net change (i.e. reference sediment production rate) for each period by the total surface occupied by badlands in the entire basin. As stated, the reference sediment production rate is the average between the two study badlands; however, in order to characterize the full spectrum of sediment production rates, the maximum and the minimum values were also used. Note that these extreme values (i.e. minimum and maximum) correspond to the values measured in the two badlands; for instance, if the sediment production in Badland #1 is less than in Badland #2 then value of Badland #1 is taken as the minimum while the value of the Badland #2 is taken as the maximum. Average surface net changes (m year^{-1}) were multiplied by the area of the badlands (m^2), and transformed to sediment production (t year^{-1}) using a bedrock density of 2.61 t m^{-3} reported by López-Tarazón et al. (2012) for badlands in the neighbouring Isábena catchment with the same lithology.

3.1.3. Discharge and suspended sediment transport at the basin outlet

Water depth and suspended sediment transport were monitored continuously in the gauging section located at the catchment outlet (see location in Figure 1). Water depth (*h*) was measured with capacitive water stage sensors/loggers (TruTrack WT-HR®) at 5-minute intervals and subsequently converted to a discharge (*Q*) using the formula for open rectangular-notch weirs to derive the *h*/*Q* relation (see Figure 1D). Suspended sediment transport was also recorded at a 5-minute interval as turbidity using an ANALITE® NEP9350® turbidity probe attached to a Campbell CR200® data logger. The range of the probe was 0-3000 NTU, equating to approximately 0-3 g l^{-1}. Turbidity values (NTU) were subsequently converted to suspended sediment concentrations (SSC) using water samples (n = 110; SSC = 0.014 x NTU – 0.80; R^2 = 0.87). Samples were obtained using a 1.7 m water stage sampler with a bottle spacing of 5 cm (i.e. one sample every 5 cm water stage increment; designed and built following the model originally developed by Schick, 1967). Samples were filtered by means of 45 μm pore cellulose filters. When concentrations were >2 g l^{-1} samples were decanted (i.e. samples were left immobile until sediments settled and the water was extracted from the samples) then oven-dried, and weighed to determine the suspended sediment concentration (SSC). The turbidity sensor was not able to measure the whole sediment concentration range, which eventually attained 10 g l^{-1} during floods. The out-of-range periods were thus derived from the SSC extracted from the samples obtained by the water stage sampler (i.e. one sample every 5 cm stage increment). Linear interpolation between sampled-based SSCs was performed to extract a SSC value per each value of flow (i.e. 5-minute data).

3.2. Data analysis

A total of 23 variables were derived from meteorological (*n* = 8), discharge (*n* = 9) and sediment records (*n* = 6) in order to first search for statistical relationships that help explain the sediment yield of the catchment and the contribution of badlands to it (see Table 2 for a complete description of the variables and their units). Meteorological variables include rainfall and temperature. The selection of variables was informed by the observation that low temperatures and rainfall are the main drivers of weathering and erosion processes in badlands areas respectively (e.g. Yair et al., 1980; Clotet et al., 1987; Gallart et al., 2002). We define a flood as a hydrological event in which discharge exceeded 1.5 times the base flow at the beginning of the rainfall (e.g. García-Ruiz et al., 2005; López-Tarazón et al., 2010; Tuset et al., 2016). Sediment production variables are estimated for all the badland surfaces in the study catchment, obtained using the reference sediment production rates measured in the experimental badlands (section 3.1.2) and the total area of the study catchment occupied by badlands.

Normality of the study variables was evaluated using the Shapiro-Wilk test (Royston, 1982). Results indicated that 6 variables (i.e. 26% of the total variables used) were not normally distributed (i.e. *p*-value > 0.01). In this way, the non-parametric Spearman's Rank correlation coefficient was used instead a Pearson correlation matrix. The analysis was performed for each of the study periods (*n* = 6) to investigate statistical correlations between variables. A *p*-value of 0.05 was set to consider the relations statistically significant, while correlations at a *p*-value smaller than 0.01 were highlighted to indicate the strongest correlations.

After the evaluation of the correlation coefficients, a backward stepwise multiple regression was applied. Variables calculated from the sediment transport observations with a high and significant correlation (i.e. >0.4) were considered as dependent variables (i.e. *SY*, SSC_{max}, SSC_m, SP_{mean}), while those calculated from the meteorological and discharge observations were considered as the independent variables (i.e. *TR*, *RD*, *MRI*, *MaxRI*, *MT*, *Zd*, *MTZD*, *MinTZD*, *R*, Q_m, *RC*, *DR*, *NF*, Q_{ci}, *FD*, Q_{mf}, *FI*). Stepwise multiple regressions allow the most influential meteorological and discharge variables on sediment transport variables to be determined. The stepwise procedure is guided by a F-value. This value indicates, for a given variable, its statistical significance in the discrimination process between groups. In our case, a F-value of 5 was set as a threshold for significance following López-Tarazón et al. (2010), Estrany et al. (2010) and more recently Tuset et al. (2016). The multiple regression analysis was performed with the seasonal data. In order to evaluate the prediction of the multivariate regression model (i.e. model goodness) data for one of the seasons (i.e. 17% of total) were randomly excluded from the multivariate analyses and used as a validation data set.

4. RESULTS

Figure 2 shows temperature, rainfall, discharge and suspended sediment transport for the whole study period. Visual relations between variables can be observed. For instance winter registered the lowest temperatures and precipitation, with consequently fewer floods and low suspended sediment concentrations; in turn, the spring and autumn periods (the latter including most of the summer season) registered the highest temperatures and rainfall which resulted in a higher occurrence of floods and largest suspended sediment concentrations. Mean annual temperature (*MT*) ranged between 12 and 13 ºC. Maximum temperature was registered during August of 2016 (i.e. 42ºC) while the minimum was recorded in January 2017 (i.e. -10ºC). A total of 61 floods were registered (22 in 2016-17 and 39 in 2017-18), with peak flows (Q_{ci}) ranging from 4.3 to 16 m^3 s^{-1}. Mean peak flow (Q_{mf}) for the entire period was 1.3 m^3 s^{-1}. Maximum registered SSC was 118.1 g l^{-1} (SSC_{max}), with a mean flood-based SSC of 7.8 g l^{-1} (SSC_{mean}). Annual rainfall (*TR*) varied between 818 and 1001 mm. Maximum intensity (*MaxRI*) was registered during June of 2017 (i.e. 24 mm h^{-1}).

4.1. Temperature, rainfall and discharge

Table 3 presents temperature, rainfall and discharge variables measured in the Soto catchment in each of the study periods. In summary, the highest mean temperature (*MT)* was registered during A2017 and A2016, whereas W2018 registered the highest *Zd* and W2017 recorded the lowest mean of minimum temperatures of days <0ºC (*MTZD)* and the absolute minimum temperature (*MinTZD)*. Regarding rainfall, maximum total rainfall (*TR)* and rainfall duration (*RD)* were registered during S2018, while maximum values of mean rainfall intensity (*MRI*) and maximum rainfall intensity (*MaxRI*) were registered in W2018 and S2017, respectively; maximum rainfall typically occurs in autumn. At the annual scale, both study periods (i.e. 2016-17 and 2017-18) presented higher rainfall than the long term mean annual rainfall (i.e. 755 mm, period 1981-2018), indicating that the study period can be considered wet in general. More specifically, 2017-18 was wetter and cooler than 2016-17, while 2016-17 was closer than the long term average value (Table 3), registering more extreme rainfall events (*MaxRI*) in all seasons, and lower minimum temperatures (*MinTZD*). Conversely, discharge variables do not show clear seasonal patterns. Instead, W2018 and S2018 presented the highest values of runoff (*R*), mean discharge (Q_m), runoff coefficient (*RC*), number of floods (*NF*) and flood duration (*FD*). In contrast, A2017 showed the highest percentage of time with the channel dry (*DR*; almost 60%). This period also presented the highest flashiness index (*FI*). Finally, A2016 registered the highest peak discharges, both maximum instantaneous flood (Q_{ci}) and mean flood discharge (Q_{mf}). At the annual scale discharge variables during 2017-18 were double the 2016-17 values, including maximum discharges, thereby highlighting the higher hydrological variability of this second study year.

Figure 3 shows the results of the Spearman's Rank correlation matrix between discharge, rainfall and temperature variables highlighting in bold the statistically significant correlations. The number of surveyed days (*ND*) is positively related with mean rainfall intensity (*MRI*), while maximum rainfall intensity of rainfall (*MaxRI*) is positively related with mean temperature (*MT*) and inversely related with days with temperature <0ºC (*Zd*). Temperature variables, as expected, show significant correlations between each other. Runoff (*R*) presented a high positive relation (p-value < 0.01) with mean discharge (Q_m), runoff coefficient (*RC*), number of floods (*NF*), and it is inversely correlated with flashiness (*FI*). Mean discharge (Q_m) presented a positive relationship with runoff coefficient (*RC*) and number of floods (*NF*). Runoff coefficient (*RC*) is positively related with total rainfall (*TR*), days with temperature <0ºC (*Zd*), number of floods (*NF*) and flood duration (*FD*), and it is inversely related with mean temperature (*MT*), mean of minimum temperatures of days <0ºC (*MTZD*), percentage of time with the channel dry (*DR)* and flashiness (*FI*). *FI* also presented a positive and strong relationship with the percentage of time with the channel dry (*DR)* and it is inversely correlated with runoff (*R*), indicating that drier periods have a lower runoff but have a higher rate of flow increase when a flood occurs. Furthermore, total rainfall (*TR*) is positively related with total runoff (*R*), mean discharge (Q_m) and runoff coefficient (*RC*), while maximum rainfall intensity (*MaxRI*) is inversely related with flood duration (*FD*). In turn, *FD* presented negative and positive relations with maximum rainfall intensity (*MaxRI*) and runoff coefficient (*RC*), respectively. Overall, *FI* shows the strongest relation with other variables, notably *MT*, *MTZD*, *MinTZD, RC* and *DR*.

4.2. Sediment production from badlands

Net changes from the two badlands ranged between 0.07 and 0.13 cm ha^{-1}. Mean annual sediment production was 0.07 cm ha^{-1} in 2016-17 and 0.10 cm ha^{-1} in 2017-18 (i.e. the complete analysis of the spatio-temporal changes on sediment erosion and export from these two experimental badlands, together with the study of the main geomorphic process signatures responsible for these, is presented in Llena et al., under revision). Table 4 summarises the sediment production from badlands in the Soto catchment for the whole study period. The highest values of sediment production from badlands were measured during spring and autumn periods (which includes most of the summer months), while the minimum values were registered during winter. These patterns are similar to those observed for sediment yield variables (see section 4.3 below). More specifically, the highest maximum sediment production (SP_{max}) and mean sediment production (SP_{mean}) were registered in A2017 while the highest minimum sediment production (SP_{min}) was measured in S2017. The minimum values were measured during W2018. At the annual scale, both years presented similar values, being SP_{mean} and SP_{max} slightly higher during 2017-18. In turn, SP_{min} was higher during 2016-17.

The Spearman's Rank correlation coefficients show several statistically significant relations (Figure 3); SP_{mean} is the sediment production variable that exhibits the strongest relationships with the meteorological and hydrological variables, followed by SP_{max}. SP_{mean} is positively related with *MTZD*, Q_{ci}, *Fi and* SP_{max}, and is negatively related with *Zd*. In turn, SP_{max} presented positive relations with *DR*, Q_{ci} and *FI*. SP_{min} in turn did not present any significant statistical relation. Results of the multiple regression analysis (Table 5) confirm the correlations obtained in the Spearman's Rank correlation analysis. In general, the significance of the meteorological variables, and more specifically low temperature, on controlling the sediment production, is remarkably high. In this way, *Zd*, *MTZD*, and *MinTZD* control the 98 % of the variability of the SP_{mean}, with the mean temperature of the days below 0ºC (*MTZD*) exhibiting the greatest weight in the model fit.

4.3. Catchment sediment yield

Table 6 summarises the catchment sediment yield for each study period. The highest values of sediment yield (*SY*), specific sediment yield (*SSY*), maximum suspended sediment concentration (SSC_{max}) and mean suspended sediment concentration (SSC_m) are registered during spring and autumn, while the lowest values are recorded in winter. At the annual scale, 2017-18 presents the highest values of sediment transport (the wettest year), except for the maximum suspended sediment concentration, which was registered in 2016-17, when the maximum rainfall intensity was also observed as indicated above.

According to the Spearman's Rank correlation coefficient results (Figure 3), overall, specific sediment yield (*SSY*) is positively related with rainfall duration (*RD*) and sediment yield (*SY*), while maximum suspended sediment concentration (SSC_{max}) is positively related with mean temperature (*MT*) and mean *Q* of floods (Q_{mf}), and inversely correlated with days with temperatures below 0ºC (*Zd*). Mean suspended sediment concentration (SSC_m) is positively correlated with flashiness (*FI*); and Sediment Delivery Ratio (*SDR*) is correlated with mean temperatures (*MT*) and maximum suspended sediment concentration (SSC_m), and inversely correlated with days with temperatures below 0ºC (*Zd*).

Although sediment yield (*SY*) does not show any significant correlation, the stepwise multiple regression analysis (Table 5) indicates that the intensity and the mean flow of the flood (Q_{ci} and Q_{mf}), together with the % time of the channel dry (DR) explain the 96% of the total variability of the *SY* with a *p*-value of 0.02. The multivariate model for the SSC_{max} is defined by three rainfall variables, being the maximum rainfall intensity (*MaxRI*) the variable with the highest weight. Finally, the multivariate model for the mean suspended sediment concentration (SSC_m) is defined by the discharge variables of flashiness (*FI*) and mean *Q* of floods (Q_{mf}), being the first the variable with the highest weight

5. DISCUSSION

5.1. Pulses of water and sediment fluxes

Meteorological and flow variables present the most significant correlations, notably: (i) total rainfall largely explains total runoff and mean discharge, more so than rainfall intensity. These findings are in agreement with results obtained by Tuset et al. (2016) in the Ribera Salada, a catchment with a long-term record in the eastern Pyrenees with no badlands, where main land use is composed by forest. (ii) Specific sediment yield is well correlated with rainfall duration; the longer the duration of the rainfall event, the higher the sediment yield observed at the outlet of the catchment. This fact was also reported by López-Tarazón et al. (2010) in the River Isábena, a neighbouring basin with similar characteristics to our study catchment, despite its larger size and perennial flow regime. These authors emphasised that river responses are controlled by the distance between the main sediment sources (i.e. badlands) and the catchment outlet. They stated that not all sediment eroded during a given rainfall event is exported out of the catchment immediately. Thus, the longer the event, the greater the opportunity for the system to export the sediment, and hence the higher the sediment yield. Similarly, results of the multivariate analysis shows that total sediment yield is mainly explained by the peak and mean discharge of the flood events (i.e. Q_{ci} and Q_{mf}), indicating the importance of the pulses of flow in transferring the sediment. Finally, (iii) temperature-based variables influence flood duration, flashiness and sediment transport variables such as sediment production and suspended sediment concentrations. The negative relationship between temperature and flood variables can be explained by changes in surface runoff generation by the low temperatures (e.g. Ollesch et al., 2005; Gallart et al., 2008). As already reported in previous studies (e.g. Nadal-Romero and

Regüés, 2010; Llena et al., under revision), low temperatures (typically recorded in winter) lead to a reduction of the erosion processes in badlands areas in favour of weathering processes. Under such circumstances, rates of suspended sediment transport and yield decrease.

Flashiness is the flow variable that best correlates with the duration of the period in which the stream is dry, sediment production and suspended sediment concentration. Flashiness is rather pronounced in the study catchment e.g. Figure 4 shows a representative (flash) flood registered in the Soto catchment: (i) surface runoff quickly concentrates in badlands after the rainfall, which is subsequently followed by a rapid response at the catchment outlet (Q reached 3.75 m^3 s^{-1} in 15 minutes, FI = 15 m^3 s^{-1} h^{-1}); and (ii) the rapid increase of the suspended sediment concentration following runoff increase (reaching a value of almost 75 g l^{-1}), indicating that sediment was readily available in the drainage network (i.e. the channel acting as a source of sediment). In terms of the relationship between flashiness and the period when the channel remains dry (*DR*), Estrany et al. (2010) observed that during dry periods, runoff generation is limited due to the low saturation of the drainage network, and only rainfall episodes exceeding infiltration rates, thus producing *Hortonian* overland flow, are the responsible for the sudden Q increases at the catchment outlet (i.e. high flashiness caused by flash floods). In the same way, Ferreira et al. (2015) found that the main infiltration-excess overland flow registered in a peri-urban catchment with humid Mediterranean climate, was generated during rainfalls in the dry summer season probably due to the soil hydrophobicity during this season. Moreover, Batalla and Vericat (2009) explained that the increase of flashiness implies a higher rate of energy expenditure in the channel per unit time, increasing the magnitude of potential channel erosion and sediment transport, which may be directly reflected in an increase of suspended sediment concentrations if in-channel fine sediment is available, hence sediment load.

Water and sediment transfer through fluvial systems is comprised of pulses (floods); a fact that is especially evident in systems characterised by intermittent regimes under highly variable hydroclimatic conditions such as that studied here (e.g. Bull and Kirkby, 2002). The degree of connectivity between sources and sinks will depend on the availability of sediments and on the capacity of running waters to transfer them through the drainage network (e.g. Cavalli et al., 2013) that ultimately will be controlled by the flow peak but also the duration of competent flows. Sediment yield in catchments without constant base flow is more dependent on high magnitude pulses than catchments having perennial streams (e.g. Estrany et al., 2009), especially if the sediment production rates in source areas are elevated (for instance, in areas of badlands). The Soto basin represents a system with high structural connectivity, but with intermittent functional connectivity (i.e. fluxes), which is mainly controlled by pulses. Evidence of this low level of functional connectivity is provided by the absence of any correlation between sediment production and export at the seasonal scale (Figure 3). In order to understand the flashy response of these types of catchments it is important to analyse the dynamics of sediment source areas as well as to role of the drainage network in buffering the sediment load to downstream (i.e. acting as source or sink of fine sediments).

5.2. The role of badlands and land cover on catchment sediment yield

Our results indicate that both sediment production in badlands and sediment yield at the catchment outlet is very variable, with autumn and spring periods showing the highest values (Figure 5A). This fact was also observed by several authors in catchments exhibiting badlands (e.g. Regüés et al., 1995; Römkens et al., 2001; Nadal-Romero et al., 2007; Lana-Renault and Regüés 2009; Nadal-Romero and Regüés, 2010; López-Tarazón et al., 2011; Desir and Marin 2013; Piqué et al., 2014; Barnes et al., 2016; Vercruyse et al., 2017) and is mainly controlled by the seasonality of weathering and erosion processes, in turn controlling sediment production and yield. For instance, in the Vallcebre catchment (Southern Pyrenees), Regüés et al. (1995) described how during winter, regolith is weathered mainly by freeze-thawing processes, while during summer convective storms (included in both spring and autumn periods in this study) most of the regolith is eroded and transferred, and consequently sediment production increases. In terms of sediment yield, Lobera et al. (2016) also observed in the neighbouring River Ésera, that the highest suspended sediment loads occurred in summer and autumn, when high magnitude rainfall episodes lead to important flood events carrying large sediment loads. Similarly, Béjar et al. (2018) identified summer and autumn as the seasons with higher sediment loads for the Upper Cinca catchment (which includes the Soto study basin).

The variability of sediment production mostly depends on badland morphometric characteristics, including vegetation cover, a fact that has been widely analysed (e.g. Yair et al. 1980; Nadal-Romero et al., 2007; Vericat et al. 2014; Nadal-Romero et al 2015; Marchamalo et al. 2016; Bonetti et al., 2019; Vergari et al., 2019). For instance, Vericat et al. (2014) stated that, at the annual scale, aspect, surface roughness and slope were significant predictors of topographic change. In SE Spain, Marchamalo et al. (2016) analysed the influence of micro-topographic factors on pathways and frequency of water and sediment fluxes, which control runoff and erosion rates. In our case we use the mean rate of sediment production obtained in both badlands as a representative value for these types of surfaces throughout the basin, since it correctly represents their morphometric and vegetation variability. The use of single values to generalise to the catchment is in fact a limitation may have an influence to the results. However, it should be noted that maximum and minimum rates of sediment production were also used to search for correlations, in order to encompass the influence of a range of morphometric characteristics on the on sediment production.

Figure 5A shows the sediment production in badlands areas based on the mean value, but also the envelope defined by the minimum and maximum specific values observed during each study period, both seasonally and annually. This figure also represents the sediment yield at the Soto catchment outlet for each of the study period. Despite the fact that, as explained above, temporal trends for badland sediment production and catchment sediment yield are similar (i.e. higher rates in spring and autumn, and lower rates in winter) a mismatch between the frequency and the magnitude of sediment production and sediment yield is evident. Several periods show larger sediment yield than production (A2016, S2017, W2018, A2018; brown areas in Figure 5A), whereas others show the opposite behaviour (W2017, S2017; grey areas in Figure 5A), production higher than the yield at the outlet. Moreover, at the annual scale, sediment production in the badlands accounts for half of the sediment yield in both study periods (i.e. 55% and 46% for 2016-17 and 2017-18 respectively). It is necessary to then analyse the role of other factors that can potentially effect the production, transfer and export of sediment in the basin: (i) the role of other land uses as sediment source occupying the 75% of the catchment area; and (ii) the role of drainage network acting as sediment source/sink.

As stated, land uses of the Soto catchment are mainly forest (56%), badlands (25%) and agricultural fields (19%). Only data from two experimental badlands was available in this study. Thus, in order to analyse the potential role of non-badlands areas on sediment production in the Soto catchment, erosion values of forested (n = 43) and agricultural (n = 69) areas with similar characteristics (e.g. precipitation) were extracted from the literature, mostly from the review provided by García-Ruiz et al. (2015). These values are summarized in Table 1 in the Supplementary Materials. Values were combined following all possible combinations in order to extract a distribution of potential Sediment Production Rates (SSP) from forest and agricultural fields. An accumulated frequency distribution for each study period was calculated and presented in Figure 5B. The 50th percentile of these distributions (i.e. values associated with an accumulated frequency of 50 % of the time) was used to compute the potential sediment production from these land uses.

Figure 5C shows the total sediment production in the Soto catchment for each study period after measured values in badlands and estimated values in forests and agriculture surfaces were integrated. As stated in the results, despite representing ¼ of the catchment area badlands still produce more than half (54%) of the sediment, being the main source of sediments; however, these results are far from those reported for instance in the neighbouring Isábena basin by Lopez-Tarazón et al. (2012), where 1% of badlands surface almost accounted for all of the basin's sediment yield at the annual scale. It is worth highlighting the different catchment area of the Isábena (445 km^2) compared to the Soto, which may have a direct impact on these differences. In the same way, Nadal-Romero and Regüés (2010) stated that, for the Araguás catchment (located around 80 km west of the study area, 0.45 km^2), sediment production in badlands are of three orders of magnitude higher than the values observed in other land uses in the same catchment.

5.3. Temporal dynamics of sediment transport

The analysis of the relationship between sediment production and sediment yield at the seasonal scale permits us to infer the sediment transfer dynamics within the catchment. Moreover, the seasonal scale helps to identify temporal trends related to the main characteristics of the meteorological variables within each season. Figure 5D illustrates the relation between total sediment production and sediment yield in the Soto catchment, which shows a double clockwise-loop with different consecutive phases: (i) exhaustion; (ii) inactivity; (iii) recharge; (iv) inactivity; and (v) exhaustion. During the first exhaustion phase (i), sediment export at the outlet changed from a high value in A2016 to a low value in W2017, while sediment production remained more or less constant. From W2017 to S2017, although the sediment yield at the outlet increased, this was not substantial and can be considered as a phase of inactivity since sediment production remained constant. Phase (ii) was related to the low occurrence of erosive meteorological events during the winter months, as well as the low availability of sediment after previous exhaustion. In phase (iii), from S2017 to A2017, the system was recharged following intense sediment production and low sediment yield at the outlet, i.e. produced sediments were not exported. Again, Phase (iv), from A2017 to W2018, represented a period of inactivity mainly due to the low occurrence of erosive meteorological events and the low and constant sediment yield at the outlet. Finally, phase (v), from S2018 to S2018, was characterized by a high sediment export (sediment yield increased more than order of magnitude) as a response to the high availability of sediment in the catchment due to the previous recharge period (iii), as well as to the high production during that period.

In the case of the neighbouring Isábena catchment, López-Tarazón et al. (2011) and Piqué et al. (2014) observed that fine sediment in the drainage network has a mean residence time of around 1 year, which corroborates the high network connectivity and the role of base flows allowing continuous sediment transfer. In contrast, continuous sediment transfer was not observed in the Soto owing to its intermittent character. More recently, Keesstra et al. (2019) observed that clockwise-loops could be explained by the temporal storage of sediment along the drainage system due to its morphological complexity as well as to in-stream vegetation structures, which could act as disconnecting landscapes features. The latter process seems not to be in operation in the Soto catchment although no data are available to investigate this fully; however, we next discuss the potential role of the stream network in buffering the sediment yield and modulating the sediment export at the catchment outlet based on our observations.

5.4. Sediment delivery and the role of the channel as sediment buffer

Throughout the study period, rates of sediment production and yield are not synchronised except for S2017. This variability is presented graphically in Figure 6A. Sediment production and export values for each period are indicated in each compartment (i.e. each study period). When the compartment is coloured in red, it indicates that the export is higher than the production, that is a sediment delivery ratio (SDR) >1. When the compartments are blue the export is smaller than the production and the SDR is <1 (Figure 6B). Finally, when the SDR is 1 the compartment is coloured grey. SDR is subjected to two main sources of uncertainty: (i) the uncertainty in the methods used for the quantification of sediment yield (e.g. Regüés and Nadal-Romero, 2013; Vercruysse et al., 2017); and/or (ii) the uncertainty associated to the estimation of sediment production from topographic changes (e.g. Smith and Vericat, 2015; James et al., 2017), or, in the particular case of this study the estimates obtained from the literature. Despite these, the observed cycles and the hysteretic behaviour (that correlate with meteorological variables), point to role of the channel network as an important role in the regulation of sediment transfer. The channel network is acting as sediment sink (transient storage) for periods with SDR <1 in which sediment production is higher than the yield (W2017, A2017 and W2018 in Figure 6B), while it is acting as sediment source when SDR>1 (A2016, S2017 and S2018 in Figure 6B).

Sediment storage can be characterized, for instance, from the study of functional sediment connectivity through the use of tracers (i.e. fingerprinting). For instance, by using lead-210 (^{210}Pbex) in catchments draining badlands in NE of Spain, Moreno-de las Heras et al. (2018) observed how bare surfaces were weathered in winter and eroded during spring-autumn.

Moreover, they reported a high connectivity between the badlands, the streams and the catchment outlet for fine sediments, and much lower connectivity for coarser sediments, which remained in the stream bed for longer periods. Jantzi et al. (2017), using volumetric changes in the channel network (i.e. repeated topographic surveys), reported sediment residence times of around 3 years in badland catchments in the South of France, mainly controlled by the degree of confinement of the stream network. In the Central Pyrenees, several authors (e.g. López-Tarazón et al., 2011; Gallart et al., 2013; Piqué et al., 2014; Buendia et al., 2015) observed that the residence time of the produced sediments is around 1 year (i.e. annually, the SDR equals 1). They also concluded that the sedimentary cycles along the catchment are not hydraulically driven, but directly driven by the amount of sediments available in the riverbed mainly controlled by sediment supply from badlands. In the case of the Soto, and given its particular physiographic characteristics (e.g. highly coupled drainage network), sedimentary dynamics (i.e. intermittent sediment production), and the flashy character of the river, we argue that the drainage network acts alternatively as sediment source or sink according to the supply of sediments from the catchment, and the magnitude and frequency of the hydrological pulses.

Besides sediment conveyance, the channel network can also act as an important sediment source through river bed erosion and transport. Gaspar et al. (2019) and Lizaga et al. (2019) stated using fingerprinting methods in Mediterranean catchments of NE Spain that the river channel can contribute up to 90% of the sediment exported during exceptional rainstorm events. Similarly, Kronvang et al. (2013) observed that bank erosion was the dominant sediment source (>90%) in the River Odense (Denmark). Despite the fact that events recorded in the Soto cannot be considered as extreme events, we hypothesise that SDR fluctuations may be in some cases explained by the succession of aggradation and degradation cycles in the channel network. The area of the fluvial channel network in the Soto is estimated at 6.25 ha by the digitalization of an orthophotomosaic of 0.5 m resolution of the study area obtained in 2015 (Spanish National Centre of Geographic Information, CNIG). Taking this into account and considering a sediment density of 2.61 t m^{-3}, the maximum negative net difference of -8237 t measured for S2018 (Figure 6B) could be balanced by a mean degradation rate of 0.13 m in the channel network (without considering contributions form bank erosion), which seems a plausible value of *fluvial* activity. Similarly, a mean net difference of -1949 t for the whole study period (i.e. 2016-18) would require a mean channel degradation of 0.03 m, which again seems to be a feasible value. These values are in agreement with erosion rates measured by Llena et al. (under revision) in the channel bottom of the experimental badlands for the same study period, which grants further support to our hypothesis of the active role of stream bed as sediment sink and source.

5.5. The sediment budget of the Soto catchment

The sediment budget of the Soto catchment for the period 2016-18 is constructed from the following elements: (i) estimation of erosion in badlands from high temporal and spatial resolution topographic surveys; (ii) estimation of erosion from other land uses from a broad systematic literature review in similar hydro climatic areas, and (iii) seasonal and annual suspended yield (export) for the whole catchment (i.e. sediment output) based on continuous SSC and *Q* data. The estimates of (i) and (ii) constitute the sediment input (sediment source) to the system. The compiled sediment budget allows the construction of a quantitative framework to infer the role of the channel network as a sediment buffer (sink and source dynamics). Sediment input for the whole period 2016-18, reaches 9250 t y^{-1}, whereas sediment output amounted to 11225 t y^{-1} (which equates to a SDR = 1.2), altogether yielding a sediment deficit of 1979 t y^{-1} for the entire basin, which we attribute to the role of the channel network supplying fine sediment.

SDR observed in the Soto is higher (i.e. >1) in comparison with catchments with similar characteristics (e.g. Walling et al., 1983; de Vente et al., 2007) a fact that, additional to the source of uncertainty already discussed above, could be due to: (i) the relatively low erosional rates from badlands (i.e. around 1 mm y^{-1} on average) in comparison to catchments in the same mountain region (i.e. from 5 to 30 mm y^{-1}; e.g. Clotet et al., 1988; Gallart et al., 2002; Nadal-Romero et al., 2007; Vericat et al., 2014); and (ii) the role of the intermittent stream and its flashiness behaviour, a fact that may exert an effect on the magnitude and frequency on the catchment sediment export. Intermittency poses a challenge in terms of the minimum time need to completely characterize a full sedimentary cycle in such type of small basins (for instance, in our case the study period is two years that were characterized by hydroclimatic values above the mean, i.e. wetter and cooler). Flashiness implies a high erosive potential in the main channel during floods, which suggest a relatively higher rate of sediment contribution (e.g. Kronvang et al., 2013; Gaspar et al., 2019) in comparison to streams where there is constant flow, that in turn controls in-channel sediment storage and depletion. It is worth noting that, as stated in section 5.2, badland morphometry has a direct effect on the sediment production, which could also modify the proposed sediment budget for the catchment. For instance, the use of the maximum sediment production rates in the two experimental badlands would drop SDR to 0.9, similar to the value reported by López-Tarazón et al. (2012) for the neighbouring Isábena catchment. Altogether, although the change on the SDR is not extremely high, reinforces the need to take into account the effects of morphometry on erosion processes in dryland and semiarid areas, and on the other, to account for the errors associated with techniques used to estimate rates of sediment production.

6. CONCLUSIONS

This paper has analysed the sediment production and the sediment yield of a small mountain catchment characterised by patchy badlands and drained by intermittent streams at multiple temporal scales. The main conclusions can be drawn as follows:

1. Meteorological and discharge variables exhibit the most significant correlations. Flashiness is the discharge variable that best correlates with the duration of the period in which the stream is dry, the sediment production and the suspended sediment concentration. Sediment yield is well correlated with rainfall and flood duration.
2. Statistically significant multivariate models exist between sediment production and transport, and meteorological and discharge based variables, respectively, being sediment production determined mainly by the low temperatures variables and sediment transport by rainfall and high flows variables.
3. Despite being the main source of sediments, badlands do not always control the export of sediments, confirming our initial hypothesis.
4. Sediment production of the two studied badlands is relatively low when compared to catchments with similar characteristics, a fact that can be attributed to their size, the method used to monitor topographic changes and the higher degree of compactness of the materials. Moreover, the badlands examined herein exhibit highly complex and spatially variable geomorphic processes, of lower magnitude when compared with badlands in other sub-humid Mediterranean areas.
5. There exists a fluctuation of the functional connectivity of the channel network caused by water and sediment pulses during flashy floods and the intermittent character of the stream.
6. The drainage network acts as a temporally variable sediment source and sink. This situation, driven by the frequency and magnitude of the water and sediment pulses, will dictate changes in sediment delivery at the catchment outlet, depending on whether the drainage network acts as a sediment sink (i.e. SDR < 1) or sediment source (i.e. SDR > 1).

Acknowledgments

This research was carried out within the framework of two research projects funded by the Spanish Ministry of Economy and Competitiveness and the European FEDER funds: MORPHSED (CGL2012-36394) and MORPHPEAK (CGL2016-78874-R). The first author has a grant funded by the Spanish Ministry of Education Culture and Sports (FPU016/01687). The fourth author is a Serra Húnter Fellow at the University of Lleida. The first, second and the fourth authors are part of the Fluvial Dynamics Research Group-RIUS, which is a Consolidated Group recognized by the Generalitat de Catalunya (2017 SGR 459645). We also acknowledge the support of the CERCA Program of the Generalitat de Catalunya. Finally, we also thank the British Society for Geomorphology to support the long-term geomorphological monitoring program in the experimental badland that started in 2013; and the members of the Fluvial Dynamics Research Group for their assistance during the fieldwork campaigns.

References:

Alatorre LC, Beguería S, Lana-Renault N, Navas A, García-Ruiz JM. 2012. Soil erosion and sediment delivery in a mountain catchment under scenarios of land use change using a spatially distributed numerical model. *Hydrology and Earth System Sciences* 16: 1321-1334.

Barnes N, Luffman I, Nandi A. 2016. Gully erosion and freeze-thaw processes in clay-rich soils, northeast Tennessee, USA. *GeoResJ* 9-12: 67-76.

Batalla RJ, Vericat D. 2009. Hydrological and sediment transport dynamics of flushing flows: implications for management in large Mediterranean rivers. *River Research and Applications.* 25: 297-134.

Béjar M, Vericat D, Batalla RJ, Gibbins CN. 2018. Variation in flow and suspended sediment transport in a montane river affected by hydropeaking and instream mining. *Geomorphology*. 310: 69-83.

Benito G, Gutiérrez M, Sancho C. 1992. Erosion rates in badland areas of the Central Ebro basin (NE-Spain). *Catena* 19: 269-286.

Bonetti S, Richter DD, Porporato A. 2019. The effect of accelerated soil erosion on hillslope morphology. *Earth Surface Processes and Landforms*.

Borrelli P, Robinson DA, Fleischer LR, Lugato E, Ballabio C, Alewell C, Meusburger K, Madugno S, Schütt; Ferro V, Bargarello V, Van Oost K, Montanarella L, Panagos P. 2013. An assessment of the global impact of 21st century land use change on soil erosion. *Nature Communications.* DOI: 10.1038/s41467-017-02142-7

Borrelli P, Marker M, Panagos P, Schutt B. 2014. Modeling soil erosion and river sediment yield for an intermountain drainage basin of the Central Apennines, Italy. *Catena* 114: 45-58.

Brasington J, Rumsby B, McVey R, 2000. Monitoring and Modelling Morphological Change in a Braided Gravel-Bed River Using High Resolution GPS-Based Survey. *Earth Surface Processes and Landforms* 25: 973-990.

Brasington J, Vericat D, Rychkov I. 2012. Modelling river bed morphology, roughness, and surface sedimentology using high resolution terrestrial laser scanning. *Water Resources Research*. 48: 1-18.

Buendia C, Vericat D, Batalla RJ, Gibbins CN. 2016. Temporal dynamics of sediment transport and transient in-channel storage in a highly erodible catchment. *Land Degradation and Development.* 27: 1045-1063.

Bull LJ, Kirkby MJ. 2002. *Dryland Rivers: Hydrology and Geomorphology of Semi-arid Channels*. John Wiley & Sons, New York. 398 pp.

Casalí J, Gastesi R, Álvarez-Mozos J, De Santisteban LM, Lersundi JDV, Giménez R, Larrañaga A, Goñi M, Agirre U, Campo MA, López JJ, Donézar M. 2008. Runoff, erosion, and water quality of agricultural watersheds in central Navarre (Spain). *Agricultural Water Management* 95 (10): 1111-1128.

Casalí J, Giménez R, De Santisteban L, Álvarez-Mozos J, Mena J, Del Valle de Lersundi J. 2009. Determination of long-term erosion rates in vineyards of Navarre (Spain) using botanical benchmarks. *Catena* 78: 12-19.

Cavalli M, Trevisani S, Comiti F, Marchi L. 2013. Geomorphic assesment of spatial sediment connectivity in small Alpine catchments. *Geomorphology*. 188: 31-41.

Cerovski-Darriau C, Roering JJ. 2016. Influence of anthropogenic land-use change on hillslope erosion in the Waipaoa River Basin, New Zealand. *Earth Surface Processes and Landforms.* 41: 2167-2176.

Chambers BJ, Garwood TWD. 2000. Monitoring of water erosion on arable farms in England and Wales. 1990-1994. *Soil Use and Management* 16: 93-99.

Clotet N, Gallart F, Sala M. 1987. Los badlands: características, interés teórico, dinámica y tasas de erosión. *Notes de Geografía Física* 15-16: 28-37.

Clotet-Perarnau N, Gallart F, Balasch JC. 1988. Medium-term erosion rates in small scarcely vegetated catchment in the Pyrenees. *Catena Supplement* 13: 37-47.

Cui Y, Parker G, Lisle TE, Gott J, Hansler-Ball ME, Pizzuto JE, Allmendinger NE, Reed JM. 2003. Sediment pulses in mountain rivers: 1. *Experiments. Water Resources Research*. 39(9): 1239-1251.

Desir G, Marín C. 2013. Role of erosion processes on the morphogenesis of a semiarid badland area. Bardenas Reales (NE Spain). *Catena* 106: 83-92.

Djorovic, M. 1992. Soil erosion problem in Yugoslavia (Republics: Serbia, Bosnia-Herzegovina, Macedonia and Montenegro). In: Safley, M., Várallyay, G., (Eds.), *Soil Erosion Prevention and Remediation Workshop*, US–Central and Eastern European Agro-Environmental Program, Budapest, Hungary. 158-174 pp.

Erskine WD, Saynor MJ. 1996. Success of soil conservation works in reducing soil erosion rates and sediment yields in central eastern Australia. In: *Erosion and Sediment Yield: Global and Regional Perspectives* (Proceedings of the Exter Symposium, July 1996). IAHS Publ. 236. 523-530 pp.

Erskine WD, Mahmoudzadeh A, Myers C. 2002. Land use effects on sediment yields and soil loss rates in small basins of Triassic sandstone near Sydney, NSW, Australia. *Catena* 49: 271-287.

Estrany J, Garcia C, Batalla RJ. 2010. Suspended sediment transport in a small Mediterranean agricultural catchment. *Earth Surface Processes and Landforms*. 34: 929-940.

Estrany J, Garcia C, Batalla RJ. 2010. Hydrological response of a small Mediterranean agricultural catchment. *Journal of Hydrology*. 380: 180-190.

Ferreira CSS, Walsh RPD, Steenhuis TS, Shakesby RA, Nunes JPN, Coelho COA, Ferreira AJD. 2015. Spatiotemporal variability of hydrologic soil properties and the implications for overland flow and land management in a peri-urban Mediterranean catchment. *Journal of Hydrology*. 525: 249-263.

Francke, T. 2009. Measurement and Modelling of Water and Sediment Fluxes in Meso-Scale Dryland Catchments. PhD thesis, Universität Potsdam, Germany. http://opus.kobv.de/ubp/volltexte/2009/3152/.

Gallart F, Solé A, Puigdefàbregas J, Lázaro R. 2002. Badland Systems in the Mediterranean. In: *Dryland Rivers: Hydrology and Geomorphology of Semi-arid Channels*. Bull LJ, Kirkby MJ (Eds.). John Wiley & Sons, Ltd. 299-326.

Gallart F, Llorens P. 2004. Observations on land cover changes and water resources in the headwaters of the Ebro catchment, Iberian Peninsula. *Physics and Chemistry of the Earth*. 29: 769–773.

Gallart F, Amaxidis Y, Botti P, Canè G, Castillo V, Chapman P, Froebrich J, García-Pintado J, Latron J, Llorens P, Lo Porto A, Morais M, Neves R, Ninov P, Perrin JL, Ribarova I, Skoulikidis N, Tournoud

MG. 2008. Investigating hydrological regimes and processes in a set of catchments with temporary waters in Mediterranean Europe. *Hydrological Sciences Journal*. 53(3): 618-628.

Gallart F, Marignani M, Pérez-Gallego N, Santi E, Maccherini S. 2013. Thirty years of studies on badlands, from physical to vegetational approaches. A succinct review. *Catena* 106: 4-11.

Gallart F, Pérez-Gallego N, Latron J, Catari G, Martínez-Carreras N, Nord G. 2013b. Short- and long-term studies of sediment dynamics in a small humid mountain Mediterranean basin with badlands. *Geomorphology* 196: 242-251.

García-Ruiz JM. Arnáez J, Beguería S, Seeger M, Martí-Bono C, Regüés D, Lana-Renault N, White S. 2005. Runoff generation in an intensively disturbed, abandoned farmland catchment, Central Spanish Pyrenees. *Catena*. 59: 79-92.

García-Ruiz JM, Regüés D, Alvera B, Lana-Renault N, Serrano-Muela P, Nadal-Romero E, Navas A, Latron J, Martí-Bono, Arnáez J. 2008. Flood generation and sediment transport in experimental catchments affected by land use changes in the central Pyrenees. *Journal of Hydrology*. 356: 245-260.

García-Ruiz JM, Beguería S, Nadal-Romero E, González-Hidalgo JC, Lana-Renault N, Sanjuán Y. 2015. A meta-analysis of soil erosion rates across the world. *Geomorphology*. 239: 160-173.

Gaspar L, Lizaga I, Blake WH, Latorre B, Quijano L, Navas A. 2019. Fingerprinting changes in source contribution for evaluating soil response during an exceptional rainfall in Spanish pre-Pyrenees. *Journal of Environmental Management*. 240: 136-148.

Geilhausem M, Otto JC, Morche D, Schrott L. 2012. Decadal sediment yield from an Alpine proglacial zone inferred from reservoir sedimentation (Pasterze, Hohe Tauern, Austria). In: *Erosion and Sediment Yield in the Changing Environment*. IAHS Publ. 356. 161-172 pp.

Giménez R, Casalí J, Díez J. 2012. Evaluación de la producción de sedimentos y calidad de las aguas en cuencas agrarias de Navarra. *Cuadernos de Investigación Geográfica* 38 (1): 7-25.

Giménez R, Casalí J, Grande I, Díez I, Díez J, Campo MA, Álvarez-Mozos J, Goñi M. 2012. Factors controlling sediment export in a small agricultural watershed in Navarre (Spain). *Agricultural Water Management* 110, 1-8.

Giménez-Morera A, Ruiz-Sinoga JD, Cerdà A. 2010. The impact of cotton geotextiles on soil and water losses in Mediterranean rainfed agricultural land. *Land Degradation and Development* 21: 210-217.

Gran KB, Czuba JA. 2017. Sediment pulse evolution and the role of network structure. *Geomorphology*. 277: 17-30.

Helming K. Prasad SN. 2002. Soil erosion under different rainfall intensities, surface roughness, and soil water regimes. *Catena* 46(2-3): 103-123.

James MR, Robson S, Smith, MW. 2017. 3-D uncertainty-based topographic change detection with structure-from-motion photogrammetry: precision maps for ground control and directly georeferenced surveys. *Earth Surface Processes and Landforms* 42: 1769–1788.

Jantzi H, Liébault F, Klotz S. 2017. Sediment residence time in alluvial storage of black marl badlands. *Catena*. 156: 82-91.

Junk JW, Bayley PB, Sparks RE. 1989. The flood pulse concept in river flood plain systems. *Can. Spec. Publ. Fish. Aquat. Sci*. 106: 110–121.

Keesstra SD, Davis J, Masselink RH, Casalí J, Peeters ETHM, Dijksma R. 2019. Coupling hysteresis analysis with sediment and hydrological connectivity in three agricultural catchments in Navarre, Spain. *Journal of Soils and Sediments*. 19:1598-1612.

Khanchoul K, Boukhrissa ZE, Acidi A, Altschul R. 2012. Estimation of suspended sediment transport in the Kebir drainage basin, Algeria. *Quaternary International* 262: 25-31.

Kronvang B, Andersen HE, Larsen SE, Audet J. 2013. Importance of bank erosion for sediment input, storage and export at the catchment scale. *Journal Soils Sediments*. 13: 230-241.

Kuo CW, Brierley GJ. 2013. Importance of bank erosion for sediment input, storage and export at the catchment scale. *Geomorphology*. 180: 255-266.

Lana-Renault N, Regüés D. 2009. Seasonal patterns of suspended sediment transport in an abandoned farmland catchment in the Central Spanish Pyrenees. *Earth Surface Processes and Landforms*. 34: 1291-1301.

Lane SN, Westaway RM, Hicks DM. 2003. Estimation of Erosion and Deposition Volumes in a Large, Gravel-Bed, Braided River Using Synoptic Remote Sensing. *Earth Surface Processes and Landforms* 28: 249-271.

Lizaga I, Gaspar L, Blake W, Latorre B, Navas A. 2019. Fingerprinting changes of source apportionments from mixed land uses in stream sediments before and after an exceptional rainstorm event. *Geomorphology*. https://doi.org/10.1016/j.geomorph.2019.05.015

Llena M, Smith MW, Wheaton JM, Vericat D. Under revision. Multi-temporal geomorphic processes reshaping sub-humid Mediterranean badlands. *Earth Surface Processes and Landforms.*

Llorens P, Gallart F, Cayuela C, Roig-Planasdemunt M, Casellas E, Molina AJ, Moreno-de Las Heras M, Bertran G, Sánchez-Costa E, Latron J. 2018. What have we learnt about Mediterranean catchment hydrology? 30 years observing hydrological processes in the Vallcebre research catchments. *Geographical Research Letters*. 44(2): 475-502.

Lobera G, Batalla RJ, Vericat D, López-Tarazón JA, Tena A. Sediment transport in two mediterranean regulated rivers. *Science of the Total Environment*. 540: 101:113.

López-Tarazón JA, Batalla, RJ, Vericat D, Balasch JC. 2010. Rainfall, runoff and sediment transport relations in a mesoscale mountainous catchment: The River Isábena (Ebro basin). *Catena*. 82: 23-34.

López-Tarazón JA, Batalla RJ, Vericat D. 2011. In-channel sediment storage in a highly erodible catchment: the River Isábena (Ebro Basin, Southern Pyrenees). *Zeitschrift für Geomorphologie*. 55(3): 365-382.

López-Tarazón JA, Batalla RJ, Vericat D, Francke T. 2012. The sediment budget of a highly dynamic mesoscale catchment: the river Isábena. *Geomorphology* 138: 15–28.

MacDonough OT, Hosen JD, Palmer M. 2011. Temporary streams: The hydrology, Geography and ecology of non-perennially flowing water. In: *River ecosystems: Dynamics, management and conservation*. Elliott, H. and Martin, L. (eds). Nova Scotia Publishers. 259-289 pp.

Marchamalo M, Hooke JM, Sandercocket PJ. 2016. Flow and sediment connectivity in semi-arid landscapes in SE Spain: patterns and controls. *Land Degradation and Development* 27: 1034-1044.

Marchi L, Borga M, Preciso E, Gaume E. 2010. Characterisation of selected extreme flash floods in Europe and implications for floods risk management. *Journal of Hydrology* 394(1-2): 118-133.

Martínez-Casasnovas JA, Poch RM. 1998. Estado de conservación de los suelos de la cuenca del embalse Joaquín Costa. *Limnética* 14: 83-91.

Mathys N, Brochot S, Meunier M, Richard D. 2003. Erosion quantification in the small marly experimental catchments of Draix (Alpes de Haute Provence, France). Calibration of the ETC rainfall–runoff–erosion model. *Catena* 50: 527-548.

Mingyi F, Walling DE, Zinbao Z, Anbang W. 2003. A study on responses of soil erosion and sediment yield to closing cultivation on sloping land in a small catchment using 137Cs technique in the Rolling Loess Plateau, China. *Chinese Science Bulletin* 48 (19: 2093-2100.

Moreno-de las Heras M, Gallart F, Latron J, Martínez-Carreras N, Ferrer L, Estrany J. 2018. Testing the use of $^{210}Pb_{ex}$ to study sediment connectivity in a Mediterranean mountain basin with badlands. *Land Degradation and Development*. 29: 676-689.

Nadal-Romero E, Regüés D, Martí-Bono C, Serrano-Muela P. 2007. Badland dynamics in the Central Pyrenees: temporal and spatial patterns of weathering processes. *Earth Surface Processes and Landforms* 32: 888-904.

Nadal-Romero E, Regüés D. 2010. Geomorphological dynamics of sub-humid mountain badland areas: weathering, hydrological and suspended sediment transport processes. A case of study in the Araguás catchment (Central Pyrenees), and implications for altered hydro-climatic regimes. *Progress in Physical Geography* 34 (3): 123–150.

Nadal-Romero E, Revuelto J, Errea P, López-Moreno JI. 2015. The application of terrestrial laser scanner and SfM photogrammetry in measuring erosion and deposition processes in two opposite slopes in a humid badlands area (central Spanish Pyrenees). *SOIL* 1, 561–573.

Nadal-Romero E, Lasanta T, García-Ruiz JM. 2013. Runoff and sediment yield from land under various uses in a Mediterranean mountain area: long-term results from an experimental station. *Earth Surface Processes and Landforms* 38: 346-355.

Navas A, López-Vicente M, Gaspar L, Machín J. 2013. Assessing soil redistribution in a complex karst catchment using fallout 137Cs and GIS. *Geomorphology* 196: 231-241.

Navratil O, Esteves M, Legout C, Gratiot N, Nemery J, Willmore S, Grangeon T. 2011. Global uncertainty analysis of suspended sediment monitoring using turbidimeter in a small mountainous river catchment. *Journal of Hydrology* 398 (3-4): 246-259.

Navratil O, Evrard O, Esteves M, Legout C, Ayrault S, Némery J, Mate-Marin A, Ahmadi M, Lefèvre I, Poirel A, Bonté P. 2012. Temporal variability of suspended sediment sources in an alpine catchment combining river/rainfall monitoring and sediment fingerprinting. *Earth Surface Processes and Landforms* 37: 828-846.

Neugirg F, Stark M, Kaiser A, Vlacilova M, Della Seta M, Vergari F, Schmidt J, Becht M, Haas F. 2016. Erosion processes in calanchi in the Upper Orcia Valley, Southern Tuscany, Italy based on multitemporal high-resolution terrestrial LiDAR and UAV surveys. *Geomorphology* 269: 8–22.

Oeurng C, Sauvage S, Sánchez-Pérez JM. 2010. Dynamics of suspended sediment transport and yield in a large agricultural catchment, southwest France. *Earth Surface Processes and Landforms* 35: 1289-1301.

Passalacqua P, Belmont P, Staley DM, Simley JD, Arrowsmith JR, Bode CA, Crosby C, DeLong SB, Glenn NF, Kelly SA, Lague D, Sangireddy H, Schaffrath K, Tarboton DG, Wasklewicz T, Wheaton JM. 2015. Analyzing high resolution topography for advancing the understanding of mass and energy transfer through landscapes: a review. *Earth-Science Reviews* 148: 174-193.

Pimentel D, Harvey C, Resosudarmo P, Sinclair K, Kurz D, McNair M, Crist S, Shpritz L, Fitton L, Saffouri R, Blair R. 1995. Environmental and Economic Costs of Soil Erosion and Conservation Benefeits. *Science*. 179: 1117-1123.

Piqué G, López-Tarazón JA, Batalla RJ. 2014. Variability of in-channel sediment storage in a river draining highly erodible areas (the Isábena, Ebro basin). *Journal Soils Sediments* 12: 2031-2044.

Porto P, Walling DE. 2012. Validation the use of 137Cs and 210Pbex measurements to estimate rates of soil loss from cultivated land in southern Italy. *Journal of Environmental Radioactivity* 106: 47-57.

Puigdefabregas J, Sole A, Gutierrez L, del Barrio G, Boer M. 1999. Scales and processes of water and sediment redistribution in drylands: results from the Rambla Honda field site in Southeast Spain. *Earth-Sci. Rev*. 48: 39–70.

Regüés D, Pardini G, Gallart F. 1995. Regolith behavior and physical weathering of claey mudrock as dependent on seasonal weather conditions in a badland area at Vallcebre, Eastern Pyrenees. *Catena* 25: 199-212.

Regüés D, Nadal-Romero E. 2013. Uncertainty in the evaluation of sediment yield from badland areas: Suspended sediment transport estimated in the Araguás catchment (central Spanish Pyrenees). *Catena* 106: 93-100.

Richard D, Mathys N. 1999. Historique, contexte technique et scientifique des BVRE de Draix. In: N. Mathys (Ed.), *Caractéristiques, données disponibles et principaux résultats acquis au cours des dix ans de suivi*. Actes du séminaire Les bassins versants expérimentaux de Draix. Cemagref-Editions, Coll. Actes de colloques, Grenoble, 11-28 pp.

Rodríguez-Blanco ML, Taboada-Castro MM, Taboada-Castro MT. 2013. Linking the field to the stream: Soil erosion and sediment yield in a rural catchment, NW Spain. *Catena* 102: 74-81.

Rodríguez-Blanco ML, Taboada-Castro MM, Palleiro L, Taboada-Castro MT. 2010. Temporal changes in suspended sediment transport in an Atlantic catchment, NW Spain. *Geomorphology* 123: 181-188.

Rossi RK. 2018. *Evaluation of `Structure-from-Motion' from a Pole-Mounted Camera for Monitoring Geomorphic Change*. Master Dissertation. Utah State University. 211 pp.

Rovira A, Batalla RJ. 2006. Temporal distribution of suspended sediment transport in a Mediterranean basin: The Lower Tordera (NE Spain). *Geomorphology* 79: 58-71.

Royston P. 1982. An extension of Shapiro and Wilk's W test for normality to large samples. *Applied Statistics* 31: 115–124.

Römkens MJM, Helming K. Prasad SN. 2002. Soil erosion under different rainfall intensities, surface roughness, and soil water regimes. *Catena* 46(2-3): 103-123.Rychov I, Brasington J, Vericat D. 2012. Computational and methodological aspects of terrestrial surface analysis based on point clouds. *Computers and Geosciences* 42:64–70.

Schick AP. 1967. Gerlach troughs, overland flow traps. Field methods for the study of slope and fluvial processes. *Revue de Géomorphologie Dynamique* 4: 170–172.

Shao Q, Xiao T, Liu JY, Qi Y. 2011. Soil erosion rates and characteristics of typical alpine meadow using 137Cs technique in Qinghai-Tibet Plateau. *Chinese Science Bulletin* 56 (16): 1708-1713.

Shao Y, Lunetta RS, Macpherson J, Luo J, Chen G. 2013. Assessing Sediment Yield for selected watersheds in the Laurentian Great Lakes Basin Under Future Agricultural Scenarios. *Environmental Management* 51: 59-69.

Smith MW, Vericat D. 2015. From experimental plots to experimental landscapes: topography, erosion and deposition in sub-humid badlands from Structure-from-motion photogrammetry. *Earth Surface Processes and Landforms* 40: 1656-1671.

Stöcker C, Eltner A, Karrasch P. 2015. Measuring gullies by synergetic application of UAV and close range photogrammetry — a case study from Andalusia, Spain. *Catena* 132: 1–11.

Surian N, Righini M, Lucía A, Nardi L, Amponsah W, Benvenuti M, Borga M, Cavalli M, Comiti F, Marchi L, Rinaldi M, Viero A. 2016. Channel response to extreme floods: Insights on controlling factors from six mountain rivers in northern Apennines, Italy. *Geomorphology* 272, 78-91.

Sutherland RA, Bryan RB. 1991. Sediment budgeting: A case study in the Katiorin drainage basin, Kenya. *Earth Surface Processes and Landforms* 16: 383-398.

Tarolli P, Borga M, Morin E, Delrieu G. 2012. Analysis of flash flood regimes in the North-Western and South-Eastern Mediterranean regions. *Natural Hazards and Earth System Sciences*. 12: 1255- 1265.

Tarolli, P. 2014. High-resolution topography for understanding Earth surface processes: opportunities and challenges. *Geomorphology* 216: 295–312.

Turnage KM, Lee SY, Foss JE, Kim KH, Larsen IL. 1997. Comparison of soil erosion and deposition rates using radiocesium, RUSLE, and buried soils in dolines in East Tennessee. *Environmental Geology* 29 (1/2): 1-10.

Tuset J, Vericat D, Batalla RJ. 2016. Rainfall, runoff and sediment transport in a Mediterranean mountainous catchment. *Science of Total Environment*. 540: 114-132.

Ollesch G, Sukhanovski Y, Kistner I, Rode M, Meissner R. 2005. Characterization and modelling of the spatial heterogeneity of snowmelt erosion. *Earth Surface Processes and Landforms*. 30: 197–211.

Porto P, Walling DE, Callegari G. 2011. Using 137Cs measurements to establish catchment sediment budgets and explore scale effects. *Hydrological Processes* 25: 886-900.

Vercruyse K, Grabowski RC, Rickson RJ. 2017. Suspended sediment transport dynamics in rivers: Multi-scale drivers of temporal variation. *Earth-Science Reviews.* 166: 38-52.

Vergari F, Troiani F, Faulkner H, Del Monte M, Della Seta M, Ciccacci S, Fredi P. 2019. The use of the slope-area function to analyse process domains in complex badland landscapes. *Earth Surface Processes and Landforms* 44: 273-286.

Vericat D, Smith MW, Brasington J. 2014. Patterns of topographic change in sub-humid badlands determined by high resolution multi-temporal topographic surveys. *Catena* 120: 164–176.

Vericat D, Wheaton J, Brasington J. 2017. Revisiting the Morphological Approach: Opportunities and Challenges with Repeat High-Resolution Topography. In: *Gravel-Bed Rivers: Processes and Disasters*. Tsutsumi DT, Laronne JB. (Eds.). Wiley, 121-158.

Walling DE. 1983. The sediment delivery problem. *Journal of Hydrology*. 65(1–3): 209–237.

Walling DE, Russell MA, Hodgkinson RA, Zhan Y. 2002. Establishing sediment budgets for two small lowland agricultural catchments in the UK. *Catena* 47: 323-353.Williams GP. 1989. Sediment concentration versus water discharge during single hydrologic events in rivers. *Journal of Hydrology* 111: 89-106.

Wheaton JM, Brasington J, Darby SE, Sear DA. 2010. Accounting for uncertainty in DEMs from repeat topographic surveys: improved sediment budgets. *Earth Surface Processes and Landforms* 35(2): 136–156.

Yair A, Lavee H, Bryan RB, Adar E. 1980. Runoff and erosion processes and rates in the Zin Valley badlands, Northern Negev, Israel. *Earth Surface Processes* 5: 205-225.

Zabaleta A, Martínez M, Uriarte JA, Antigüedad I. 2007. Factors controlling suspended sediment yield during runoff events in small headwater catchments of the Basque Country. *Catena* 71: 179-190.

FIGURE CAPTIONS

Figure 1. (A) Land cover map of the Soto study catchment in the context of the Upper Cinca basin (southern Pyrenees) and the Iberian Peninsula (inset). **(B)** Image of one of the badlands studied in this paper to estimate the overall sediment production of the rest of badland surfaces in the catchment. **(C)** General view of the middle part of the study catchment with a land cover mosaic composed by agricultural fields, badlands and forest. **(D)** Gauging station at the outlet of the catchment (channel width ≅ 14 m).

Figure 2. Variables recorded in the Soto catchment during 2016-2018. (A) Rainfall and temperature; (B) Flow discharge (*Q*); (C) Suspended sediment concentrations (*SSC*); (D) Sediment production in badlands. All variables are recorded at 5-minute intervals.

Figure 3. Spearman's Rank correlation coefficient matrix between temperature, rainfall, discharge, sediment production from badlands and catchment sediment yield for the 6 different seasonal periods analysed (see Table 2 for a description of each variable). Values in bold indicate that statistical relations are significant at $p < 0.05$, while bold and italic values indicate that relations are significant at $p < 0.01$.

Figure 4. (A) Rainfall, discharge and suspended sediment concentration measured at 5-min interval for the flash flood of 9th September 2016. (B) An area of badlands just before the onset of rainfall and (C) at the highest rainfall intensity (i.e. 6 mm in 5 minutes). (D) Gauging station located at the catchment outlet (see location in Figure 1) just before the flood started and (E) during peak *Q*. Note that (i) the rainfall gauge is located in B and C, and (ii) the time between B and C, and D and E indicates the time-lapse between both photographs were taken.

Figure 5. (A) Badlands' sediment production (grey line) and catchment sediment yield (brown line) for each study period (see section 3.1. for details). Brown areas represent the periods in which catchment sediment yield is higher than sediment production from badlands, while grey areas represent the opposite, i.e. periods in which sediment production is higher than the yield. Dotted lines represent the minimum and the maximum sediment production values registered in the two study badlands. Vertical lines represent the amplitude of the sediment production based on these extreme values. (B) Accumulated frequency distribution curves of sediment production values associated with forest and agricultural fields for each study period. These curves were estimated based on values obtained from the literature (Table 1 of supplementary materials; see section 5.2. for further details). (C) Comparison between measured sediment production in badlands (i.e. based on the mean or reference value) and estimated sediment production in agricultural and forested surfaces based on the median value (50th percentile) of the curves in B. (D) Seasonal hysteresis between sediment production and sediment yield in the Soto catchment.

Figure 6. (A) Model of in-channel sediment storage fluctuations in relation to sediment production (inputs, grey arrows) and sediment export at the catchment outlet (outputs, brown arrows). (B) Changes in the sediment delivery ratio SDR for each study period.

FIGURES

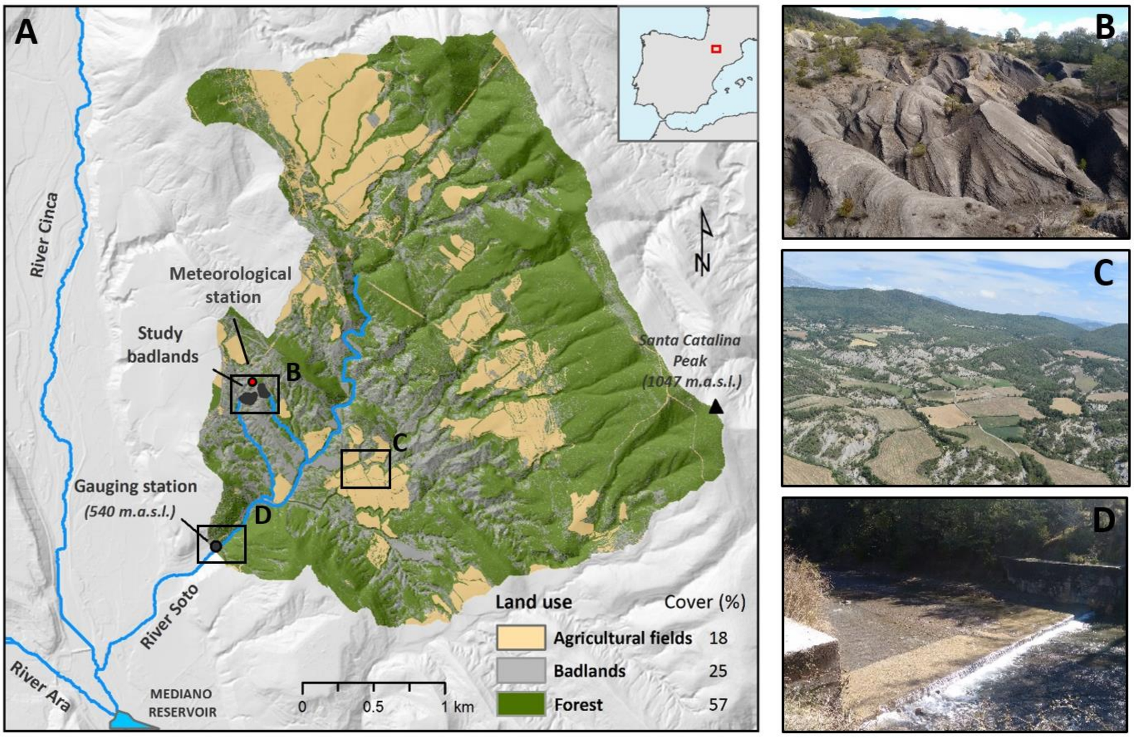

Figure 1.

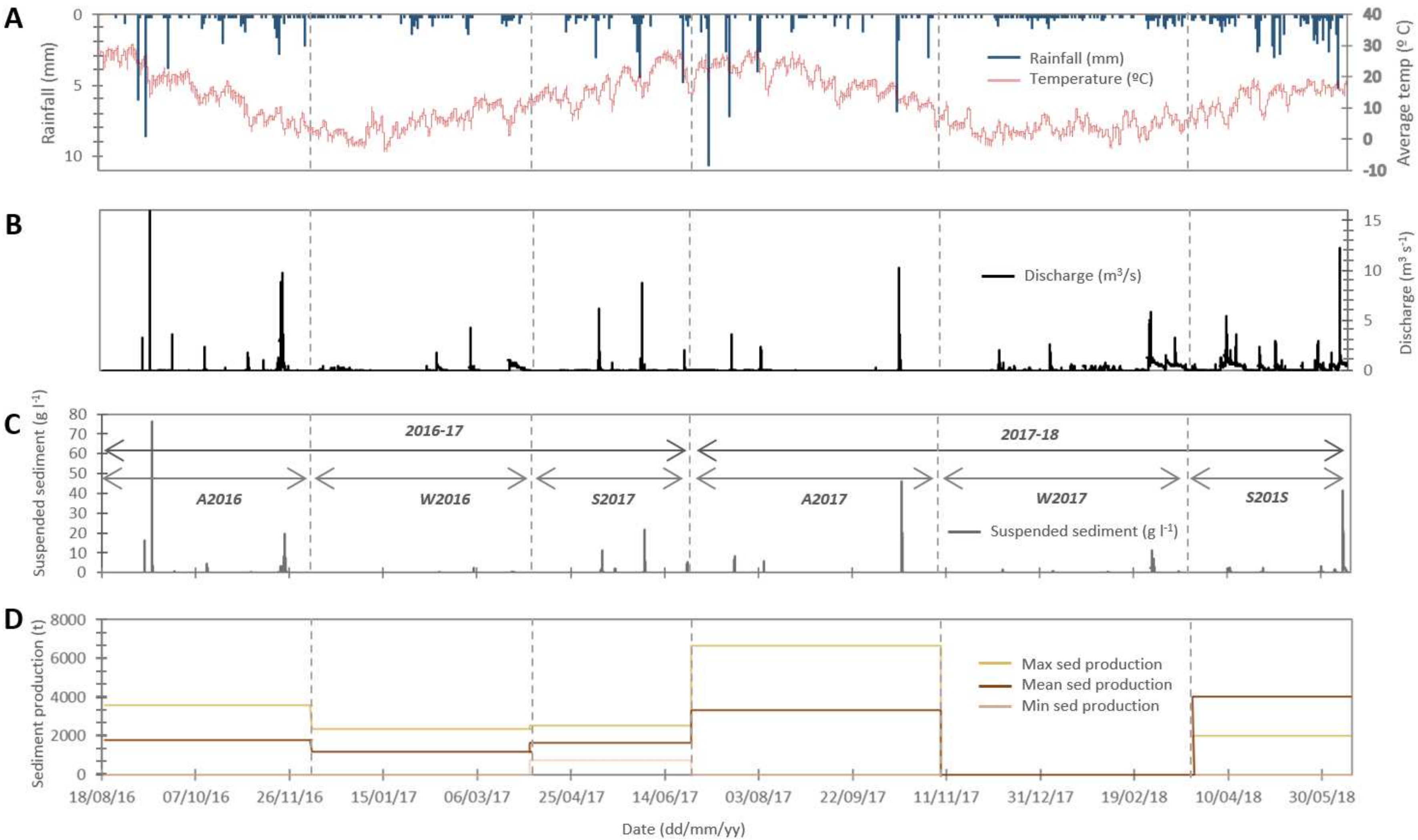
A
Rainfall (mm)
Average temp (º C)
Rainfall (mm)
Temperature (ºC)
B
Discharge (m³/s)
Discharge (m³ s⁻¹)
C
Suspended sediment (g l⁻¹)
2016-17
2017-18
A2016
W2016
S2017
A2017
W2017
S201S
Suspended sediment (g l⁻¹)
D
Sediment production (t)
Max sed production
Mean sed production
Min sed production
18/08/16
07/10/16
26/11/16
15/01/17
06/03/17
25/04/17
14/06/17
03/08/17
22/09/17
11/11/17
31/12/17
19/02/18
10/04/18
30/05/18
Date (dd/mm/yy)

Figure 2.

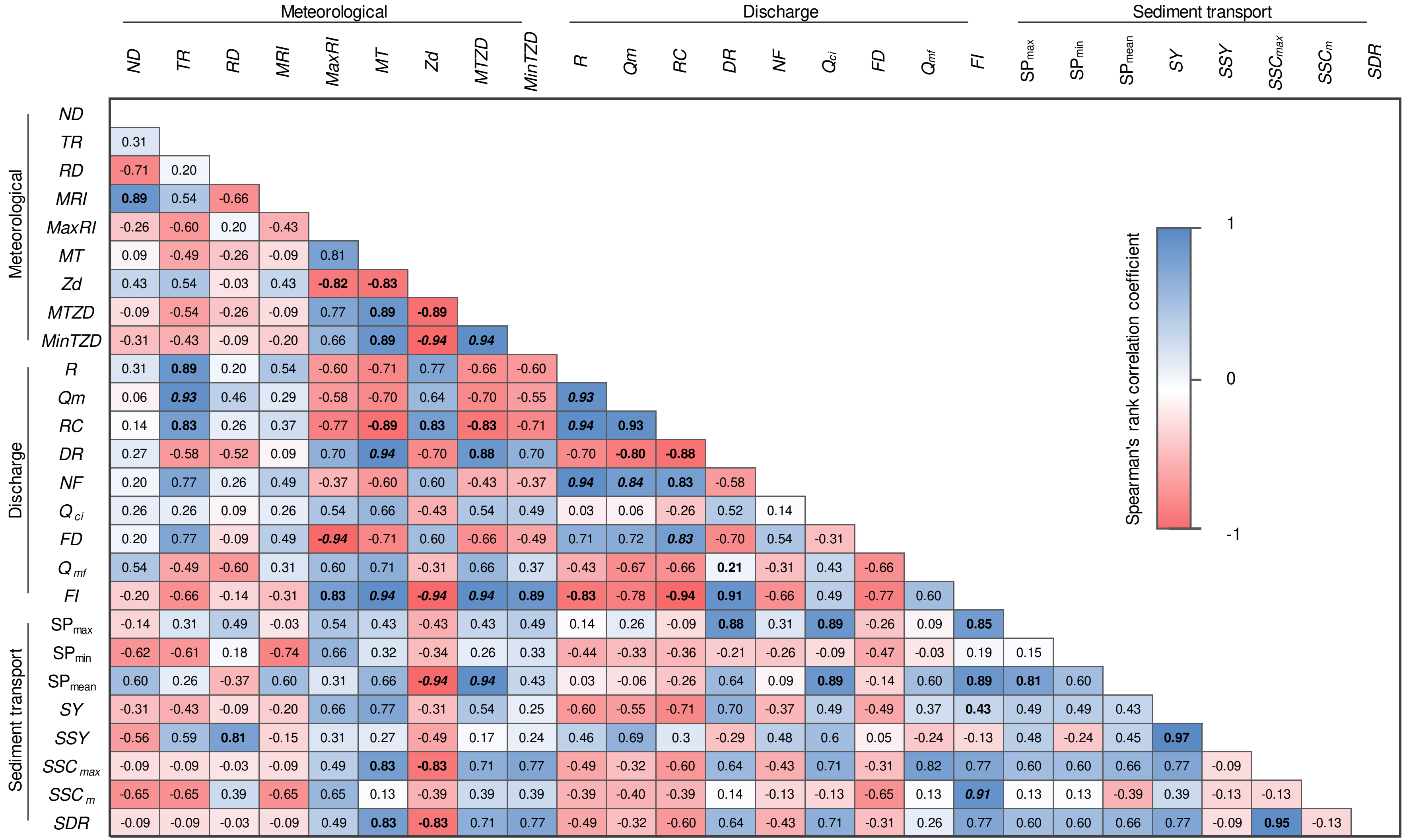
Meteorological
Discharge
Sediment transport
ND TR RD MRI MaxRI MT Zd MTZD MinTZD R Qm RC DR NF Qci FD Qmf FI SPmax SPmin SPmean SY SSY SSCmax SSCm SDR
ND
TR 0.31
RD -0.71 0.20
MRI 0.89 0.54 -0.66
MaxRI -0.26 -0.60 0.20 -0.43
MT 0.09 -0.49 -0.26 -0.09 0.81
Zd 0.43 0.54 -0.03 0.43 -0.82 -0.83
MTZD -0.09 -0.54 -0.26 -0.09 0.77 0.89 -0.89
MinTZD -0.31 -0.43 -0.09 -0.20 0.66 0.89 -0.94 0.94
R 0.31 0.89 0.20 0.54 -0.60 -0.71 0.77 -0.66 -0.60
Qm 0.06 0.93 0.46 0.29 -0.58 -0.70 0.64 -0.70 -0.55 0.93
RC 0.14 0.83 0.26 0.37 -0.77 -0.89 0.83 -0.83 -0.71 0.94 0.93
DR 0.27 -0.58 -0.52 0.09 0.70 0.94 -0.70 0.88 0.70 -0.70 -0.80 -0.88
NF 0.20 0.77 0.26 0.49 -0.37 -0.60 0.60 -0.43 -0.37 0.94 0.84 0.83 -0.58
Q ci 0.26 0.26 0.09 0.26 0.54 0.66 -0.43 0.54 0.49 0.03 0.06 -0.26 0.52 0.14
FD 0.20 0.77 -0.09 0.49 -0.94 -0.71 0.60 -0.66 -0.49 0.71 0.72 0.83 -0.70 0.54 -0.31
Q mf 0.54 -0.49 -0.60 0.31 0.60 0.71 -0.31 0.66 0.37 -0.43 -0.67 -0.66 0.21 -0.31 0.43 -0.66
FI -0.20 -0.66 -0.14 -0.31 0.83 0.94 -0.94 0.94 0.89 -0.83 -0.78 -0.94 0.91 -0.66 0.49 -0.77 0.60
SPmax -0.14 0.31 0.49 -0.03 0.54 0.43 -0.43 0.43 0.49 0.14 0.26 -0.09 0.88 0.31 0.89 -0.26 0.09 0.85
SPmin -0.62 -0.61 0.18 -0.74 0.66 0.32 -0.34 0.26 0.33 -0.44 -0.33 -0.36 -0.21 -0.26 -0.09 -0.47 -0.03 0.19 0.15
SPmean 0.60 0.26 -0.37 0.60 0.31 0.66 -0.94 0.94 0.43 0.03 -0.06 -0.26 0.64 0.09 0.89 -0.14 0.60 0.89 0.81 0.60
SY -0.31 -0.43 -0.09 -0.20 0.66 0.77 -0.31 0.54 0.25 -0.60 -0.55 -0.71 0.70 -0.37 0.49 -0.49 0.37 0.43 0.49 0.49 0.43
SSY -0.56 0.59 0.81 -0.15 0.31 0.27 -0.49 0.17 0.24 0.46 0.69 0.3 -0.29 0.48 0.6 0.05 -0.24 -0.13 0.48 -0.24 0.45 0.97
SSC max -0.09 -0.09 -0.03 -0.09 0.49 0.83 -0.83 0.71 0.77 -0.49 -0.32 -0.60 0.64 -0.43 0.71 -0.31 0.82 0.77 0.60 0.60 0.66 0.77 -0.09
SSC m -0.65 -0.65 0.39 -0.65 0.65 0.13 -0.39 0.39 0.39 -0.39 -0.40 -0.39 0.14 -0.13 -0.13 -0.65 0.13 0.91 0.13 0.13 -0.39 0.39 -0.13 -0.13
SDR -0.09 -0.09 -0.03 -0.09 0.49 0.83 -0.83 0.71 0.77 -0.49 -0.32 -0.60 0.64 -0.43 0.71 -0.31 0.26 0.77 0.60 0.60 0.66 0.77 -0.09 0.95 -0.13
Spearman's rank correlation coefficient
1
0
-1

Figure 3.

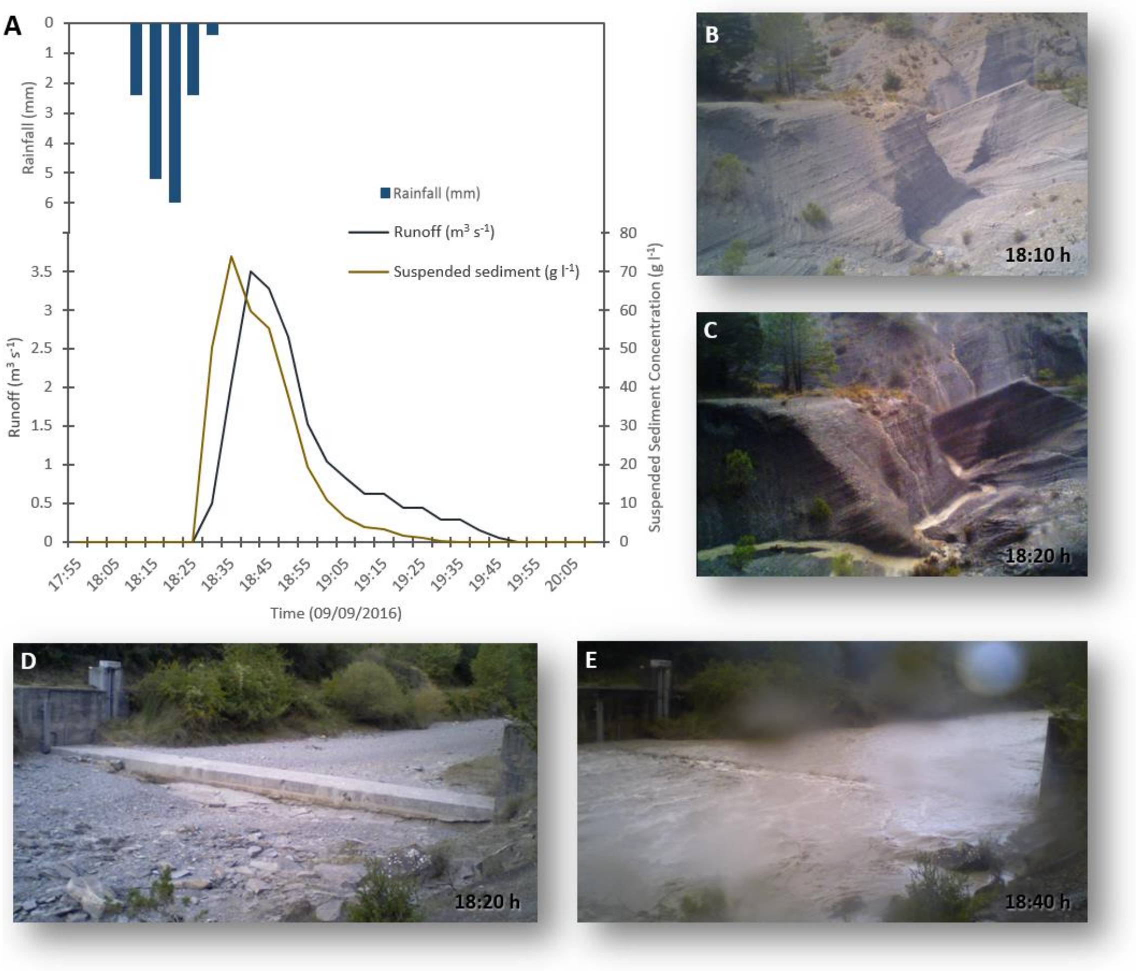
A
Rainfall (mm)
Rainfall (mm)
Runoff (m3 s-1)
Suspended sediment (g l-1)
Runoff (m3 s-1)
Suspended Sediment Concentration (g l-1)
Time (09/09/2016)
B
18:10 h
C
18:20 h
D
18:20 h
E
18:40 h

Figure 4.

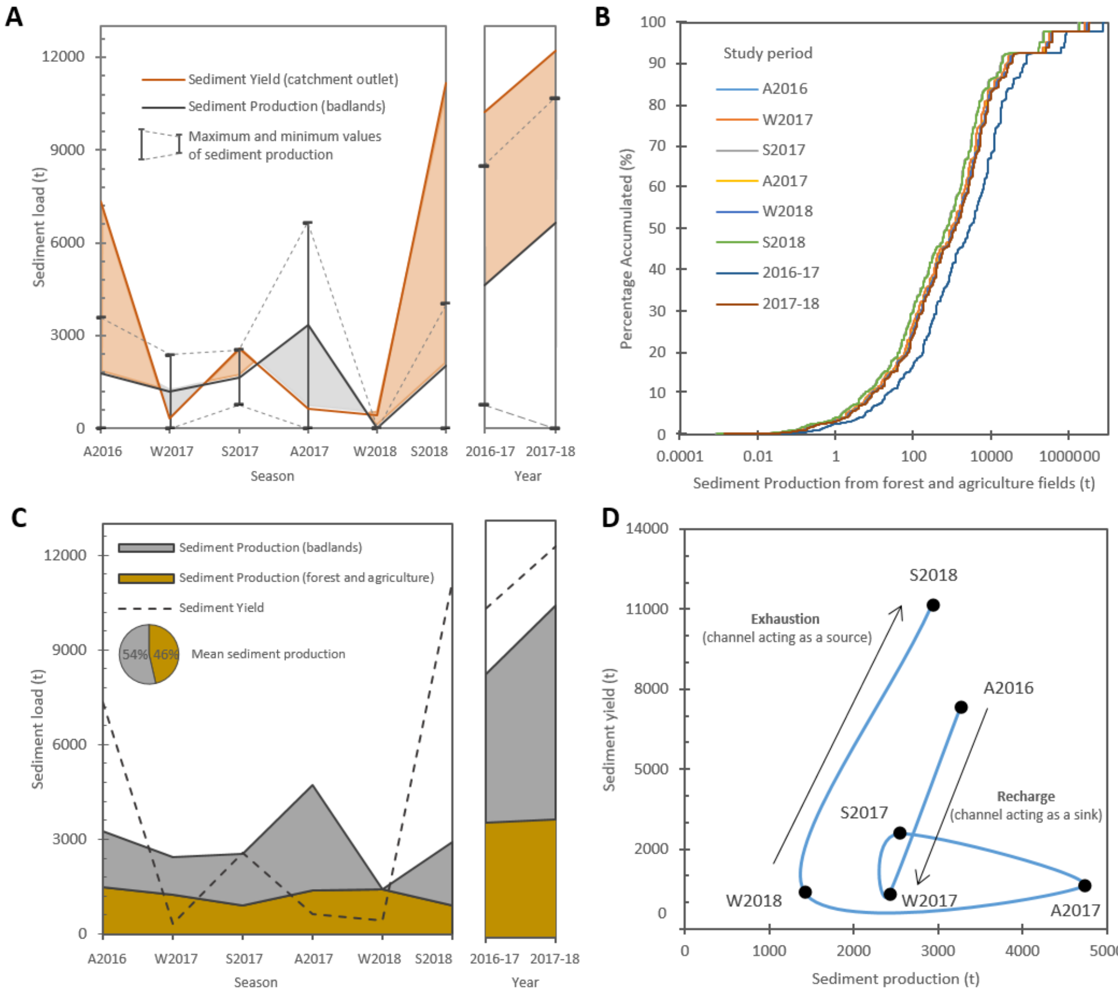

1015

1016 Figure 5.

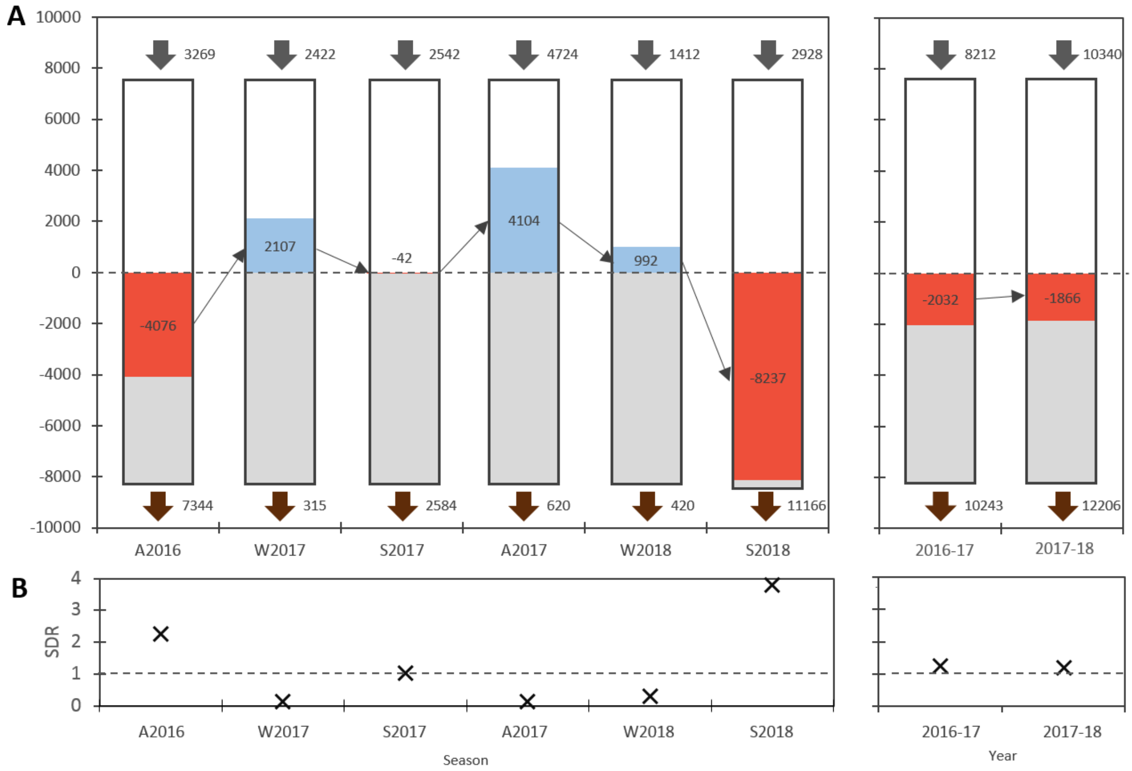
A
B
10000
8000
6000
4000
2000
0
-2000
-4000
-6000
-8000
-10000
3269
2422
2542
4724
1412
2928
8212
10340
-4076
2107
-42
4104
992
-8237
-2032
-1866
7344
315
2584
620
420
11166
10243
12206
A2016
W2017
S2017
A2017
W2018
S2018
2016-17
2017-18
SDR
4
3
2
1
0
Season
Year

Figure 6.

TABLES AND TABLES CAPTIONS

Table 1. Distribution of the study periods: starting and ending dates, called period and name.

Scale	Name[1]	Period	Study period Start	Study period End
SEASONAL	A2016	Autumn 2016	19/07/2016	07/12/2016
	W2017	Winter 2016	07/12/2016	01/04/2017
	S2017	Spring 2017	01/04/2017	28/06/2017
	A2017	Autumn 2017	28/06/2017	08/11/2017
	W2018	Winter 2017	08/11/2017	23/03/2018
	S2018	Spring 2018	23/03/2018	18/06/2018
ANNUAL	2016-17	2016-2017	19/07/2016	28/06/2017
	2017-18	2017-2018	28/06/2017	18/06/2018

[1] The year attributed to each period is the starting year (e.g. the winter between 2017 and 2018 is labelled here W2017).

Table 2. Meteorological, discharge and sediment-based variables, showing the corresponding abbreviations and measuring units.

Type of variable	Abbreviation	Description	Unit
Time	*ND*	Number of surveyed days	Day
Meteorological	*TR*	Total rainfall	mm
	RD	Rainfall duration	hour
	MRI	Mean rainfall intensity	mm $hour^{-1}$
	MaxRI	Maximum rainfall intensity	mm $hour^{-1}$
	MT	Mean temperature	ºC
	Zd	Days with temperature <0ºC	Nº of days
	MTZD	Mean of minimum temperatures of days <0ºC	ºC
	MinTZD	Absolute minimum temperature	ºC
Discharge	*R*	Runoff	hm^{-3}
	Q_m	Mean discharge	$m^3 s^{-1}$
	RC	Runoff coefficient	
	DR	% time channel dry	%
	NF	Number of floods	nº
	Q_{ci}	Maximum instantaneous flood discharge	$m^3 s^{-1}$
	FD	Flood duration	hours
	Q_{mf}	Mean flood discharge	$m^3 s^{-1}$
	FI	Flashiness Index$_1$	$m^3 s^{-1} h^{-1}$
Sediment transport	*SY*	Sediment yield	t
	SSY	Specific sediment yield	t ha^{-1} $year^{-1}$
	SSC_{max}	Maximum suspended sediment concentration	g l^{-1}
	SSC_m	Mean suspended sediment concentration	g l^{-1}
	SDR	Sediment Delivery Ratio	SY/ SP_{mean}
	SP_{min}	Minimum sediment production	t
	SP_{max}	Maximum sediment production	t

SP_{mean}	Mean sediment production	t

[1] Note that FI was estimated as the rate of increment of discharge per unit of time (as per Batalla and Vericat, 2009).

Table 3. Meteorological and discharge variables registered in the Soto catchment during 2016-2018 (see Table 2 for a description of variables). For reference, largest values of each variable are highlighted in bold.

Period		***TR***	***RD***	***MRI***	***MaxRI***	***MT***	***Zd***	***MTZD***	***MinTZD***	***R***	***Q_m***	***RC***	***DR***	***NF***	***Q_{ci}***	***FD***	***Q_{mf}***	***FI***
		mm	*hour*	mm $hour^{-1}$	mm $hour^{-1}$	*ºC*	*Nº of days*	*ºC*	*ºC*	hm^3	$m^3 s^{-1}$		%	*Nº*	$m^3 s^{-1}$	*hour*	$m^3 s^{-1}$	$m^3 s^{-1} h^{-1}$
SEASONAL	**A2016**	355	163.4	2.17	20.4	18.2	13	-1.35	-4.19	0.94	0.09	0.26	21	9	**16.0**	172.0	**2.22**	3.43
	W2017	254	171.3	1.49	10.2	5.1	70	**-3.28**	**-9.89**	0.92	0.09	0.36	0	6	4.3	641.8	0.82	0.96
	S2017	209	185.0	1.13	**24.6**	17.1	3	-1.06	-2.16	0.47	0.06	0.22	4	7	8.8	122.3	1.25	4.62
	A2017	246	117.5	2.09	17.4	**19.0**	0	-	-	0.34	0.03	0.14	**58**	4	10.3	174.8	1.88	**8.70**
	W2018	362	158.4	**2.29**	8.0	3.8	**102**	-2.94	-7.66	**1.84**	0.18	**0.50**	0	**18**	5.8	**975.0**	0.91	0.74
	S2018	**393**	**232.6**	1.69	16.6	13.3	7	-1.56	-3.54	1.83	**0.26**	0.46	0	17	12.2	696.7	0.63	2.51
ANNUAL	**2016-17**	818	519.7	1.57	**24.6**	**13.4**	86	-1.90	**-9.89**	2.32	0.08	0.28	8	22	**16.0**	936.1	**1.43**	3.01
	2017-18	**1001**	**550.1**	**1.82**	17.4	11.8	**109**	**-2.25**	-7.66	**4.01**	**0.16**	**0.40**	**19**	**39**	12.2	**1846.5**	1.14	**3.98**

Table 4. Sediment production from badlands registered in the Soto catchment during 2016-2018 (see Table 2 for a description of each variable). The largest values of each variable are highlighted in bold. Note that these data are extracted from Llena et al. (under revision).

Period		***SP_{min}***	***SP_{max}***	***SP_{mean}***
		t	*t*	*t*
SEASONAL	**A2016**	0	3588.3	1794.2
	W2017	0	2372.2	1186.1
	S2017	**755.4**	2541.7	1648.6
	A2017	0	**6664.8**	**3332.4**
	W2018	0	0	0
	S2018	0	4029.0	2014.5
ANNUAL	**2016-17**	**755.4**	8502.2	4628.8
	2017-18	0	**10693.8**	**5346.9**

Table 5. Results of the backward stepwise multiple regression analysis between meteorological, discharge and sediment transport variables (see Table 2 for abbreviations).

Equation	**R^2**	***p*-value**	**Model goodness**
$\boldsymbol{SP_{mean}} = 3030.99 - 12.42 \times Zd + 1474.45 \times MTZD + 356.76 \times MinTZD$	0.98	0.07	73%
$\boldsymbol{SY} = - 1774.67 + 1323.37 \times Q_{ci} - 5235.76 \times Q_{mf} - 22.38 \times DR$	0.96	0.02	81%
$\boldsymbol{SSC_{max}} = - 37.45 + 6.36 \times MaxRI + 0.38 \times TR - 0.71 \times RD$	0.89	0.06	55%
$\boldsymbol{SSC_m} = 4.77 + 2.30 \times FI - 2.47 \times Q_{mf}$	0.76	0.04	86%

Table 6. Summary of flow and sediment transport variables registered in the Soto catchment during 2016-2018 (see Table 2 for a description of each variable). The largest values of each variable are highlighted in bold. Note that flow-related variables are also included for reference.

	Period	*Flow*			*Sediment transport*			
		Q_m	*NF*	Q_{ci}	*SY*	*SSY*	SSC_{max}	SSC_m
		$m^3\ s^{-1}$	*Nº*	$m^3\ s^{-1}$	*T*	$t\ ha^{-1}\ year^{-1}$	$g\ l^{-1}$	$g\ l^{-1}$
SEASONAL	**A2016**	0.09	9	**16.0**	7344.4	7.8	**118.1**	7.8
	W2017	0.09	6	4.3	314.6	1.2	7.3	1.2
	S2017	0.06	7	8.8	2584.1	14.1	37.0	14.1
	A2017	0.03	4	10.3	620.1	**19.6**	78.5	**19.6**
	W2018	0.18	**18**	5.8	420.0	5.8	38.3	5.8
	S2018	**0.26**	17	12.2	**11165.6**	11.1	49.3	11.1
ANNUAL	**2016-17**	0.08	22	**16.0**	10243.1	7.7	**118.1**	7.7
	2017-18	**0.16**	**39**	12.2	**12205.7**	**11.6**	78.5	**12.2**

SUPPLEMENTARY MATERIAL

Table 1. References consulted to estimate specific Sediment Production Rates (SSP) in agricultural and forest areas.

Reference	**Study Area**	**Land use**	**Mean annual rainfall** (mm)	**SSP** (Mg/ha/yr)
Alatorre et al., 2010	West southern Pyrenees (Spain)	Agricultural	-	75.5000
Arthonditsis et al., 2000	Greece	Agricultural	-	0.0013
Bruggeman et al., 2005	Syrian Arab Republic	Agricultural	-	26.5500
Casalí et al., 2008	Latxaga (Spain)	Agricultural	835	0.0010
Casalí et al., 2008	Latxaga (Spain)	Agricultural	835	0.0043
Casalí et al., 2008	Latxaga (Spain)	Agricultural	835	0.0156
Casalí et al., 2008	Latxaga (Spain)	Agricultural	835	0.0203
Casalí et al., 2008	Latxaga (Spain)	Agricultural	835	0.0232
Casalí et al., 2008	La Tejería (Spain)	Agricultural	725	0.0249
Casalí et al., 2008	La Tejería (Spain)	Agricultural	725	0.1301
Casalí et al., 2008	Latxaga (Spain)	Agricultural	835	0.1362
Casalí et al., 2008	La Tejería (Spain)	Agricultural	725	0.1396
Casalí et al., 2008	La Tejería (Spain)	Agricultural	725	0.2325
Casalí et al., 2008	La Tejería (Spain)	Agricultural	725	0.2550
Casalí et al., 2008	Latxaga (Spain)	Agricultural	835	0.2628
Casalí et al., 2008	Latxaga (Spain)	Agricultural	835	0.3386
Casalí et al., 2008	La Tejería (Spain)	Agricultural	725	0.7905
Casalí et al., 2008	La Tejería (Spain)	Agricultural	725	0.8148
Casalí et al., 2008	La Tejería (Spain)	Agricultural	725	3.3189
Chahor et al., 2014	Laxaga (Spain)	Agricultural	800	0.0330
Chahor et al., 2014	Laxaga (Spain)	Agricultural	800	0.0509
Chambers and Garwood, 2000	Bollitree (England)	Agricultural	-	0.1626
Chambers and Garwood, 2000	Morfe Valley (England)	Agricultural	-	0.3673
Chambers and Garwood, 2000	Kenton (England)	Agricultural	-	0.9910
Chambers and Garwood, 2000	Llanishen (England)	Agricultural	-	1.0598
Chambers and Garwood, 2000	Ashcombe (England)	Agricultural	-	1.2097
Chambers and Garwood, 2000	Bicton (England)	Agricultural	-	1.8966
Chambers and Garwood, 2000	Starcross (England)	Agricultural	-	4.2500
Chambers and Garwood, 2000	Penalt (England)	Agricultural	-	6.8750
Dunjó et al., 2004	West southern Pyrenees (Spain)	Agricultural	-	0.5596
Erskine et al., 2002	20 (Australia)	Agricultural	1363	1.3019
Erskine et al., 2002	22 (Australia)	Agricultural	1217	3.0357
Erskine et al., 2002	10 (Australia)	Agricultural	966	16.0000
Erskine et al., 2002	11 (Australia)	Agricultural	940	22.9323
Geilhausen et al., 2012	Pasterze catchment (Austria)	Agricultural	-	0.0073
Giménez et al., 2012	La Tejería (Spain)	Agricultural	724	0.0180
Giménez et al., 2012	Latxaga (Spain)	Agricultural	830	0.0590
JRC, 2012	All Europe	Agricultural	-	9.2600
Mingyi et al., 2003	Zhaojia catchment (China)	Agricultural	528.4	25.6045
Nadal-Romero et al. 2012	West southern Pyrenees (Spain)	Agricultural	-	3.7850
Nadal-Romero et al., 2013	EEVA (Spain)	Agricultural	1216.7	841.1111
Nadal-Romero et al., 2013	EEVA (Spain)	Agricultural	1216.7	971.7778

Nobre, 2011	Northwest Portugal	Agricultural	-	0.2188
Nunes et al., 2011	Northwest Portugal	Agricultural	-	3.2395
Oeurng et al., 2010	Save catchment (France)	Agricultural	603	0.0001
Oeurng et al., 2010	Save catchment (France)	Agricultural	787	0.0006
Ordoñez-Fernández et al., 2007	South Spain	Agricultural	-	1.4000
Porto et al. 2011	Trionto (Italy)	Agricultural	-	0.0002
Porto et al. 2012	Trionto (Italy)	Agricultural	-	0.0004
Shao et al., 2013	Peshtigo River (EEUU)	Agricultural	-	0.0000
Shao et al., 2013	St. Joseph River (EEUU)	Agricultural	-	0.0000
Shao et al., 2013	St. Mary River (EEUU)	Agricultural	-	0.0000
Shao et al., 2013	Cattaraugus Creek (EEUU)	Agricultural	-	0.0003
Turnage et al. 1997	East Tennesse (EEUU)	Agricultural	1300	0.3876
Turnage et al. 1997	East Tennesse (EEUU)	Agricultural	1300	1.6524
Ursic and Dendy, 1963	Northern Mississippi (U.S.A.)	Agricultural	-	8.8021
Walling et al., 2002	New Cliftonthorp (UK)	Agricultural	644	0.0063
Walling et al., 2002	Lower Smisby (UK)	Agricultural	644	0.2715
Walling et al., 2002	Lower Smisby (UK)	Agricultural	758	0.3465
Alatorre et al., 2010	West southern Pyrenees (Spain)	Forestal	-	22.8571
Arthonditsis et al., 2000	Greece	Forestal	-	0.0002
Borrelli et al., 2014	Upper Turano River watershed (Italy)	Forestal	1205	0.0087
Bruggeman et al., 2005	Syrian Arab Republic	Forestal	-	5.1000
Djorovic, 1992	Jasenica River Basin (Serbia)	Forestal	760	0.0003
Djorovic, 1992	Jasenica River Basin (Serbia)	Forestal	760	0.0074
Djorovic, 1992	Jasenica River Basin (Serbia)	Forestal	760	0.0561
Dunjó et al., 2004	West southern Pyrenees (Spain)	Forestal	-	0.0784
Duvert et al., 2012	Cal Rodo (Spain)	Forestal	862	0.1190
Duvert et al., 2012	Ca ´'Isard (Spain)	Forestal	862	0.6769
Erskine et al., 2002	18 (Australia)	Forestal	962	4.7727
Erskine et al., 2002	15 (Australia)	Forestal	907	8.3333
Erskine et al., 2002	16 (Australia)	Forestal	1008	10.3333
Gallart et al., 2013b	Ca L'Isard (Spain)	Forestal	862	0.4444
Giménez et al., 2012	Oskotz (Spain)	Forestal	1137	0.0003
JRC, 2012	Europe	Forestal	-	0.0700
Khanchoul et al., 2012a	Wadi Cherf (Algeria)	Forestal	290	0.0001
Khanchoul et al., 2012a	Kebir (Algeria)	Forestal	700	0.0005
Khanchoul et al., 2012a	Kebir (Algeria)	Forestal	700	0.0005
Nadal-Romero et al. 2012	West southern Pyrenees (Spain)	Forestal	-	0.4150
Navas et al., 2013	Estanque de Arriba Lake (Spain)	Forestal	595	0.0000
Navratil et al., 2012	Bleéone at Chaffaut (France)	Forestal	820	0.0023
Navratil et al., 2012	Bes at Pérouré (France)	Forestal	820	0.0209
Nobre, 2011	Northwest Portugal	Forestal	-	0.0102
Nunes et al., 2011	Northwest Portugal	Forestal	-	0.0120
Ordoñez-Fernández et al., 2007	South Spain	Forestal	-	0.3000
Porto et al. 2011	Bonis (Italy)	Forestal	1250	0.0600
Porto et al. 2012	W2 (Italy)	Forestal	670	107.6605
Porto et al. 2012	W2 (Italy)	Forestal	670	47.7108
Porto et al. 2012	W2 (Italy)	Forestal	670	87.3950
Porto et al. 2012	W2 (Italy)	Forestal	670	31.8937

Porto et al. 2012	W3 (Italy)	Forestal	670	16.9118
Porto et al. 2012	W3 (Italy)	Forestal	670	11.3372
Rodríguez-Blanco et al., 2010	Corbeira (Spain)	Forestal	895	0.0034
Rodríguez-Blanco et al., 2010	Corbeira (Spain)	Forestal	1397.2	0.0069
Rodríguez-Blanco et al., 2010	Corbeira (Spain)	Forestal	1191.6	0.0054
Rovira and Batalla, 2006	Tordera (Spain)	Forestal	-	0.0004
Turnage et al. 1997	East Tennesse (EEUU)	Forestal	1300	6.5178
Turnage et al. 1997	East Tennesse (EEUU)	Forestal	1300	1.6000
Ursic and Dendy, 1963	Northern Mississippi (U.S.A.)	Forestal	-	0.2428
Walling et al., 2002	Belmont (UK)	Forestal	691	0.5347
Walling et al., 2002	Belmont (UK)	Forestal	694	0.5580
Walling et al., 2002	New Cliftonthorp (UK)	Forestal	758	1.2777
Walling et al., 2002	Jubilee (UK)	Forestal	694	2.6503
Walling et al., 2002	Jubilee (UK)	Forestal	691	5.9183
Walling et al., 2002	Moorfield (UK)	Forestal	-	10.4500
Walling et al., 2002	New Cliftonthorp (UK)	Forestal	-	14.0000
Walling et al., 2002	Foxbridge (UK)	Forestal	-	16.3390
Walling et al., 2002	Foxbridge (UK)	Forestal	-	16.5763
Walling et al., 2002	Longlands (UK)	Forestal	-	17.7931
Zabaleta et al., 2007	Aixola (Spain)	Forestal	1200	0.0365